ACS Energy LETTERS

Cite This: ACS Energy Lett. 2019, 4, 1687−1709

http://pubs.acs.org/journal/aelccp

REVIEW

2D Nanomaterials for Photocatalytic Hydrogen Production

Priyanka Ganguly,[†,‡] Moussab Harb,[§] Zhen Cao,[§] Luigi Cavallo,[§] Ailish Breen,[†,‡] Saoirse Dervin,[†,‡] Dionysios D. Dionysiou,*[,∥] and Suresh C. Pillai*[,†,‡]

[†]Nanotechnology and Bio-Engineering Research Group, Department of Environmental Science, Faculty of Science, Institute of Technology Sligo, Ash Lane, Sligo F91 YW50, Ireland

[‡]Centre for Precision Engineering, Materials and Manufacturing Research (PEM), Institute of Technology Sligo, Ash Lane, Sligo F91 YW50, Ireland

[§]KAUST Catalysis Center (KCC), Physical Sciences and Engineering Division (PSE), King Abdullah University of Science and Technology (KAUST), Thuwal 23955-6900, Saudi Arabia

[∥]Environmental Engineering and Science Program, Department of Biomedical, Chemical and Environmental Engineering (DBCEE), University of Cincinnati, Cincinnati, Ohio 45221-0012, United States

ABSTRACT: The photocatalytic water splitting technique is a promising alternative to produce hydrogen using a facile and proficient method. In the current Review, recent progress made in photocatalytic hydrogen evolution reaction (HER) using 2D nanomaterials (NMs) and composite heterostructures is described. The strong in-plane chemical bonds along with weak van der Waals interaction make these materials lucrative for surface-related applications. State-of-the-art protocols designed for the synthesis of 2D NMs is discussed in detail. The Review illustrates density functional theory (DFT)-based studies against the new set of 2D NMs, which also highlights the importance of structural defects and doping in the electronic structure. Additionally, the Review describes the influence of electronic, structural, and surface manipulation strategies. These impact the electronic structures, intrinsic conductivity, and finally output toward HER. Moreover, this Review also provides a fresh perspective on the prospects and challenges existing behind the application and fabrication strategies.

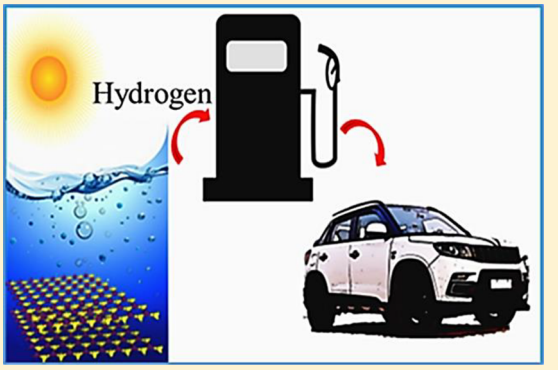

Hydrogen is considered as a clean and sustainable form of energy for the future.[1,2] The importance of hydrogen as a fuel arises due to the high yield of energy emanated upon combustion (122 kJ/mol), which far exceeds that of gasoline or any other form of fossil fuel.[3,4] This process is environmentally benign, and it does not produce any harmful byproducts.[5] At present, the process of hydrogen generation involves CO_2 production.[6,7] Therefore, searching for viable alternatives excluding the production of any greenhouse gases is the key element. Utilizing solar energy to produce photocatalytic hydrogen on the surface of a catalyst is one a promising alternative to resolve the current energy and environmental crisis.[8−10]

The photocatalytic water splitting technique is a promising alternative to produce hydrogen.

Hydrogen production ability utilizing photocatalytic materials have been demonstrated since 1972.[11] Henceforth, a multitude of semiconductor materials has been explored to evaluate their potential for hydrogen production efficiency.[12−14] The prerequisite of this search is to identify materials with optimal band structure that promotes the charge separation, simultaneously remaining stable against photocorrosion and structural stability after prolonged application. Apart from the composition and the molecular arrangement, the morphological dimension of the material contributes to the key aspect. Illuminating a photocatalytic surface with energy greater than or equal to its band gap leads to the creation of electron−hole pairs.[15] These photogenerated charge carriers produced within the nanostructure are required to react with water molecules existing on the surface. In this process of reaching the surface, the charge carriers undergo recombina-

Received: April 30, 2019
Accepted: June 11, 2019
Published: June 11, 2019

tion or get trapped at defect sites. Ida et al. effectually explained the importance of time and energy required by nanomaterials (NMs) of two different dimensions in the process of water splitting (Figure 1).[16] A nanocrystal to

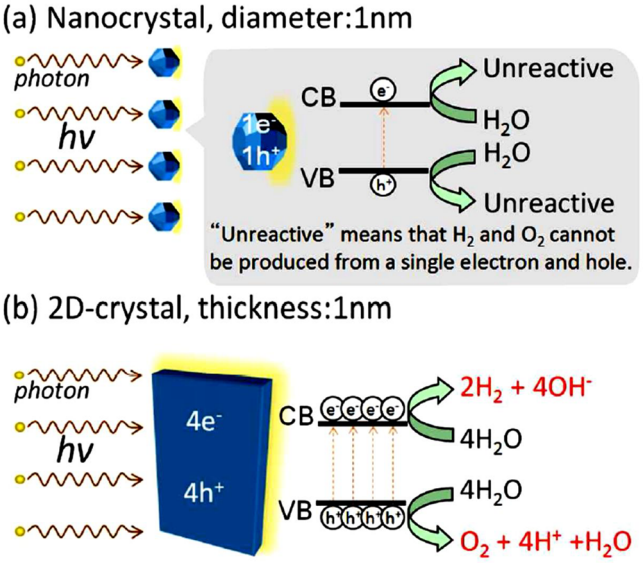

Figure 1. Schematic illustration of the photocatalytic water splitting reaction under solar light illumination for a (a) nanocrystal photocatalyst and (b) 2D photocatalyst. Reproduced with permission of ref 16. Copyright 2014, American Chemical Society.

undergo water splitting to yield hydrogen requires four electron generations and further endures a reduction of water. Thus, to produce four electrons, the nanocrystal surface is required to be impinged with four photons with appropriate energy at a short span of time. The solar photon flux density is estimated to be 2000 μmol s^{-1} m^{-2}.[15] Therefore, at least 4 ms of time is required by the photons to be absorbed by the nanoparticles, and the lifetime of the charge carriers is estimated to be 1 μs.[15] Hence, it is extremely challenging to obtain a solar energy flux to complete the water splitting reaction. In order to reduce the recombination and shorten the traveling distance for the charge carriers, two-dimensional (2D) architecture nanomaterials can serve these requirements. The layered structure aids the process of light absorption even at a low flux density, and the charge carriers generated are required to travel only a very small distance.[15,16]

The 2D materials illustrate the unique ability of confinement of electrons in their ultrathin layer, resulting in exceptional optical and electronic properties. The strong in-plane covalent bonding offers sites for the formation of numerous heterojunctions and heterostructures. Moreover, the 2D architecture boasts a high specific surface area, which enables surface reactions such as water splitting. Graphene is the first 2D material example to exhibit unique electronic, mechanical, and optical properties.[17,18] The whole graphene revolution led to an entirely new domain of research of similar structures.[19−21] 2D transition metal dichalcogenides (TMDs) have gained extensive attention in recent years. TMDs are made of hexagonal layers of metal atoms (M) squeezed in between two layers of chalcogen atoms (X) with stoichiometry MX_2.[22] The sheets are bonded together by covalent interaction, while the adjacent sheets are bonded by van der Waals interactions, resulting to form a 3D crystalline structure. There exist 40 different types of TMDs relying upon the combination of transition metals and the chalcogen atoms.[22,23] The arrangement of these atoms in the crystal structure determines the physical and chemical properties.[22,23] In the case of MoS_2, the optical and electronic properties were altered as the number of layers was reduced. It was found that MoS_2 in bulk has an indirect band gap, which transforms into a direct band gap in a few layered flakes.[24] Similarly, 2D graphitic carbon nitride (C_3N_4) is another widely investigated layered structure with remarkable electrical and optical properties.[25−27] Low-dimensional catalysts have emerged to be candidates of interest for various applications. The visible-light absorption, as well as the compatible band gap of these materials, makes them convincing candidates for H_2 production.[28,29] The electronic properties of this structure play a crucial role in underlying the catalytic reaction mechanism of these materials. The adsorption or the binding of any reactant depends on the density of the electronic structure at the Fermi level. Stronger binding is associated with the height of the center of the electronic structure relative to the energy of the Fermi level. Hence, band structure understanding is imperative for developing strategies to design effective catalysts that could essentially enhance the catalytic output.[30,31] However, there exist plausible limitations of these structures. Structural instability, high exciton recombination, poor band gap, etc. are some of the major concerns.[23] Different techniques such as the introduction of co-catalyst or doping with metals and nonmetals, surface engineering, etc. help in the reduction of the recombination rate. They also provide strategies to achieve structural stability, prevent photocorrosion, and increase visible-light absorption. These eventually lead to improvement of the photocatalytic hydrogen production output.[32−35]

Although there exist numerous reports highlighting 2D NMs, there has been a great deal of progress made in the last 5 years with respect to fabrication and improved hydrogen production.[36−38] The current Review highlights recent advances in the use of 2D NMs and their nanoheterostructure composites for photocatalytic water splitting reaction. The Review also details the commonly used synthesis methods and highlights the first-principle studies of a new class of 2D materials. An entire section has been dedicated to understanding the strategies that influence the electronic structure of these materials, which covertly influences the photocatalytic output. Finally, the Review discusses recent reports on 2D NMs used for H_2 production.

Fundamentals of Photocatalytic Hydrogen Evolution Reaction. In a critical Perspective, Teoh and co-workers outlined the very basic demand of a functioning photocatalytic system.[39] These are the following: first the ability to provide better charge transfer mobility; second, incorporation of the facile synthetic process with an efficient reaction mechanism; finally, the importance of photons to impeach the nanoarchitectures to reach the photoactive sites.[39] In this section, the basics of both photocatalysis and hydrogen production are discussed.

Photocatalysis. The search for an optimal H_2 evolution catalyst initiated as early as 1958. Parsons et al. observed that the catalytic evolution is directly linked to the formation of heat (of H_2) on the catalyst surface.[40] Moreover, using computational chemistry, Norskov and co-workers established the ability to predict the binding energies, which in turn helped in understanding the efficiency of H_2 production.[41]

DOI: 10.1021/acsenergylett.9b00940
ACS Energy Lett. 2019, 4, 1687−1709

The water splitting reaction involves two sets of basic reactions, the hydrogen evolution reaction (HER) and the oxygen evolution reaction (OER) (Figure 2).

$$2H^+ + 2e^- \rightarrow H_2 \qquad E^0 = 0.00\ V \tag{1}$$

$$2H_2O \rightarrow O_2 + 4H^+ + 4e^- \qquad E^0 = +1.23\ V \tag{2}$$

$$H_2O \rightarrow H_2 + \frac{1}{2}O_2$$

$$\Delta E^0 = 1.23\ V,\ \Delta G^\circ = +237.2\ kJ/mole \tag{3}$$

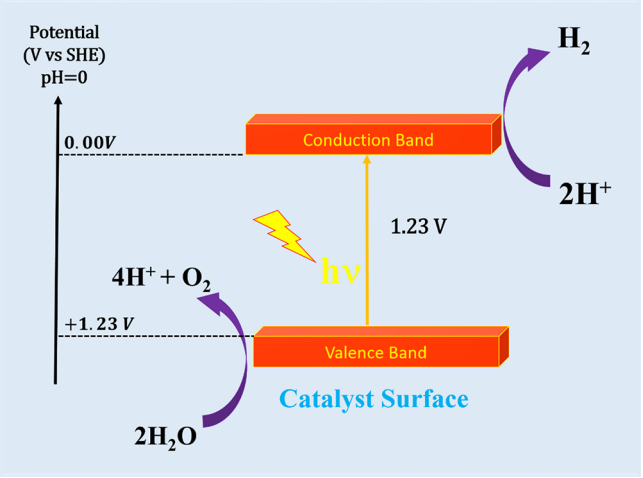

Figure 2. Schematic illustration of photocatalytic hydrogen generation on the catalytic surface sites of 2D NMs.

Hence, the whole strategy is to find out photocatalytic surfaces that have the potential to absorb light and produce electron−hole pairs. These electrons and holes can then proceed in the HER and OER reaction on the catalyst surface. However, to attain this target, it is important that the conduction band (CB) edge of the catalyst should be more negative than the reduction potential of H^+ to H_2 (0.00 V), while the valence band (VB) edge of the surface should be more positive than the oxidation potential of H_2O to O_2 (1.23 V). In summation, the band gap value of the semiconductor is estimated to be 1.23 V, but due to thermal losses, the broader approximation or suitable semiconductor band gap is in between 1.5 and 2.5 eV.

Hydrogen Evolution Reaction. The hydrogen production presently is established by steam reforming. In this process, methane reacts with steam in the presence of a catalyst at high temperature and pressure to convert into carbon monoxide and hydrogen gas. The CO generated in this step is utilized again to expose to surplus steam to attain CO_2 and more H_2.

$$CH_4 + H_2O \rightarrow CO + 3H_2 \tag{4}$$

$$CO + H_2O \rightarrow CO_2 + H_2 \tag{5}$$

The use of solar energy for water splitting reaction to generate H_2 is one of the most ecofriendly techniques. However, the use of solar energy for H_2O splitting is categorized into four types. which are discussed below.

Thermochemical Water Splitting: In this process, high temperature drawn from solar energy or waste nuclear heat is utilized to initiate a chemical reaction on the surface of a catalyst to produce hydrogen and oxygen. The high temperature (500−2000 °C) is drawn using large concentrators or using waste heat generated from advanced nuclear reactors. This water splitting process occurs in two different processes. One is the "direct" way that utilizes a two-step course. On the other hand, a more complex method is the "hybrid" process that involves multiple steps, but the operating temperature is comparatively lower than that in the direct method and involves less radiative loss.[42−44]

Photobiological Water Splitting: In this process, microorganisms such as cyanobacteria and green algae are utilized in the presence of sunlight to generate hydrogen from water.[45] These microorganisms absorb light through pigments present in two photosystems (photosystem I and photosystem II). Later, the absorbed light is transferred to the chlorophyll reaction centers, where the charge separation occurs to form different reductants and oxidants.[45−47] These reductants and oxidants react in the photosystems to generate electrons and holes, which further participate in the water splitting process. The disadvantage of this process is the low level of hydrogen produced and the low solar to hydrogen efficiency. Hence, this process is commercially unviable; however, in the near future, with searches for a zero fossil fuel society, utilization of the tiniest form of energy is advantageous.[48]

Photoelectrochemical (PEC) Water Splitting: Honda and Fujishima were the first people to report the use of TiO_2 electrodes for H_2 generation under UV light illumination.[49] Henceforth, this idea was extended toward a particulate system

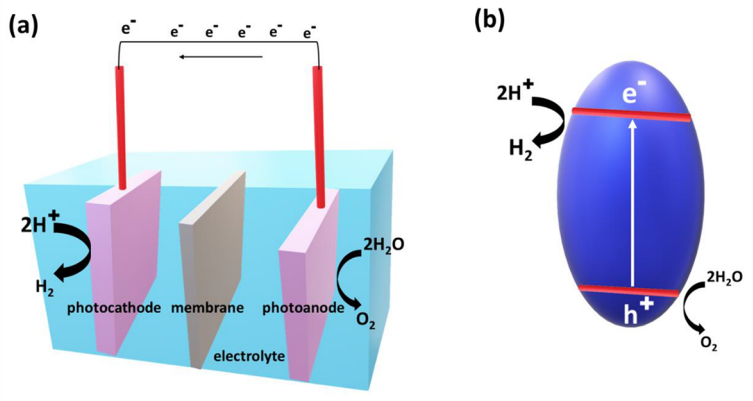

Figure 3. Schematic diagram of (a) PEC and (b) photocatalytic hydrogen generation from water splitting.

DOI: 10.1021/acsenergylett.9b00940
ACS Energy Lett. 2019, 4, 1687−1709

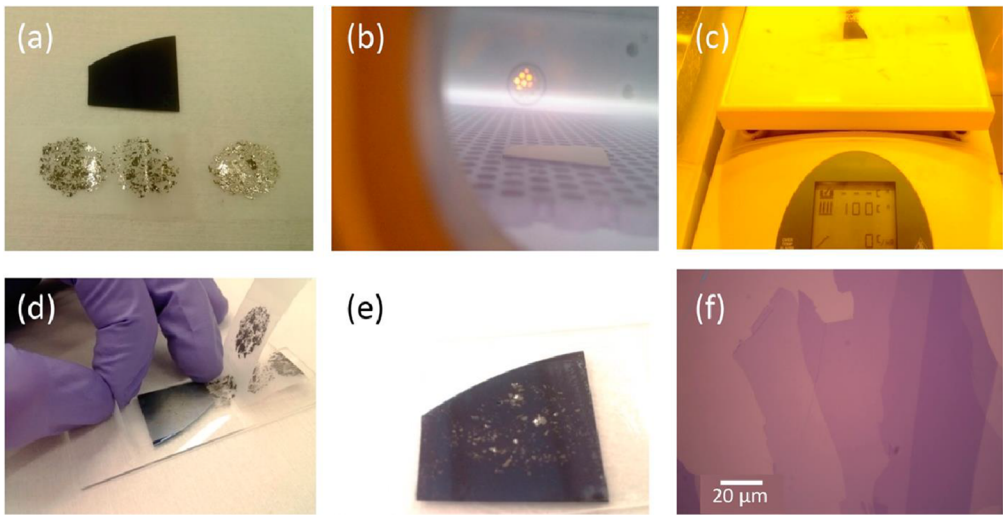

Figure 4. Illustration of the typical exfoliation process for graphene using the scotch tape method improved by the micromechanical cleavage technique. Reproduced with permission from ref 62. Copyright 2015, American Chemical Society.

in heterogeneous photocatalysis by Bard et al.[50] During the previous 50 years, significant advances were made in this field. The PEC activity of hydrogen production occurs inside of a PEC cell under light irradiation (Figure 3a). It consists of a working photoanode, which is made up of semiconductor materials for oxygen evolution, and a counter photocathode for hydrogen evolution. These electrodes are placed inside of an electrolyte solution with a wire connecting the current loop in between the electrodes to complete the circuit. Semiconductors with a band gap greater than 1.23 V can be used as photoelectrodes for hydrogen generation. This can provide an external bias to enable the reaction. However, the use of additional bias often leads to partial depletion of electrons in the semiconductor photoactive surface. This depletion results in the formation of a surface space layer and the associated band bending. This procedure necessarily decreases the rate of recombination and increases the lifespan of the charge carriers.[51]

Extensive studies highlighting the use of 2D nanostructures for electrochemical hydrogen generation have been conducted in the past decade.[52] The photocatalytic electrochemical activity and the photocatalytic water splitting reactions are measured by evaluating the amount of hydrogen or oxygen emanated from the reactions. The H_2 production rate is normally measured in μmol h^{-1} g^{-1} and the photocurrent density in mA cm^{-2}. The wavelength and intensity of the incident radiation are a few of the other parameters of concern. However, every reaction setup is different and yields varied results. Therefore, to compare the results, two parameters are used, which are known as the quantum yield (QY) or apparent quantum yield (AQY) (eqs 6–8).[53]

$$\mathrm{QY\%} = \frac{\text{Number of reacted electrons}}{\text{Number of absorbed photons}} \times 100 \tag{6}$$

$$\mathrm{AQY\%} = \frac{\text{Number of reacted electrons}}{\text{Number of incident electrons}} \times 100 \tag{7}$$

$$= \frac{\text{Number of evolved hydrogen molecules} \times 2}{\text{Number of incident photons}} \times 100 \tag{8}$$

Photocatalytic Water Splitting: In this process, a high yield of H_2 is generated by irradiating the catalyst surface with sunlight or visible light. The catalysts, or more categorically defined as photocatalysts, are the semiconductor materials aiding in the water splitting reactions without being transformed or consumed in this procedure (Figure 3b). It is a more reliable process compared to the previous options because of the huge solar to H_2 efficiency and easy operation approach. The semiconductor surface upon irradiation with sufficient energy results in the creation of electron–hole pairs. These electron–hole pairs are quite unstable and have the tendency of easy recombination. However, structural or electronic manipulation aid in transporting the charge carriers to initiate a chemical reaction on the catalyst surface. To illustrate the efficiency of the water splitting reaction under sunlight, the PEC and photocatalytic water splitting reactions are associated with another parameter for solar to H_2 conversion efficiency [STH] (eq 9) under 1.5 global (AM 1.5G) illumination.[53]

$$\mathrm{STH\%} = \left(\frac{\text{output energy of hydrogen}}{\text{energy of the incident solar light}}\right)\mathrm{AM_{1.5G}} \times 100$$

$$= \left(\frac{\text{mmoles of hydrogen/s} \times 237\ \text{kJ/mole}}{P_{\text{total}}(\text{mW/cm}^2) \times \text{Area(cm}^2)}\right)\mathrm{AM_{1.5G}} \times 100 \tag{9}$$

To enhance the H_2 production efficiency, several synthesis routes of novel materials are discussed in the latter section. The synthesis of these materials is carried out by both top-down and bottom-up approaches.

Synthesis Strategies. Significant efforts have been invested in exploring different novel routes of 2D NM synthesis.[54−56] Exfoliation of the bulk materials by retracting out from the strong interplane covalent bonding is an example of the top-down approach. On the other hand, wet chemical synthesis from its precursor stage or deposition of thin layers using a chemical vapor deposition (CVD) technique are examples of the bottom-up approach. In the present section, we aim to introduce the conventional and innovative approaches of synthesis steps attempted to produce different types of 2D NMs.

Exfoliation. This top-down synthesis approach utilizes force in the solid state with or without the use of solvents. All of the

DOI: 10.1021/acsenergylett.9b00940
ACS Energy Lett. 2019, 4, 1687−1709

crystals cannot yield bonds in three dimensions; hence, layered crystals or materials are defined as the solids with weak out-of-plane van der Waals bonding and exhibit strong in-plane chemical bonds. This allows parallel delamination, resulting in even atomically thin nanosheets from their bulk layered precursors.[57] The exfoliation process results in a broad surface area available for surface-active catalytic functions. In a broader aspect, there exist two primary methods of exfoliation; mechanical exfoliation and liquid-phase exfoliation. Generally, an external stimulus in the form of a force is exerted upon the bulk materials to cleave them into the atomically thin layer or at least into a few layered materials. This stimulus has to work against the strong in-plane bond and the weak van der Waals force functioning between the layered structures.

Mechanical Exfoliation. The mechanical cleavage of bulk layered materials, commonly referred to as the "scotch tape method", is one of the most pioneering techniques introduced by Novoselov et al. to isolate a single layer of 2D NMs.[17] The use of chemical exfoliation resulting in tampered structures with enormous defects and isolation of a single layer seemed to be a challenging task and more of a transient phase in the process. On the other hand, mechanical exfoliation was utilized as a viable technique to isolate hundreds of layers of 2D NMs. In this technique, a piece of "scotch" tape is utilized to scrape off layers of layered materials from the bulk materials. As a result, micron-sized fragments of 2D NMs are peeled off, which are subsequently transferred over substrates of silicon/silica through wet or dry transfer methods.[58−60] Gomez et al. reported the synthesis of 2D layers of BP. Unlike the conventional scotch tape method, the authors introduced intermediate viscoelastic surfaces to exfoliate the flakes, which resulted in a substantial increase of the yield and reduced the contamination of the fabricated flakes.[61] Huang et al. modified the mechanical cleaving technique by introducing a pretreatment process of the substrate with oxygen plasma, which resulted in the removal of ambient adsorbates (Figure 4). Final thermal treatment was performed to introduce exfoliation and obtain better interface contact with the substrate and the bulk crystals. This technique eventually resulted in improved surface area and increased the production yield of the nanosheets produced.[62]

Though this technique has become a fundamental means of exfoliating layered materials, it suffers from its own sets of limitations. High yield and production of sheets with controlled size and shape cannot be accomplished utilizing this technique. The need for a substrate layer in most of the cases for the exfoliated sheets is certainly another factor limiting any realistic application that requires large yield and moderately stable sheets. This technique certainly lacks these aspects, and hence, alternative approaches have been explored.

Liquid-Based Exfoliation. Similar to mechanical exfoliation, the synthesis method by exfoliating layered bulk materials in the liquid can result in the synthesis of 2D NMs. Sonication force or mechanical thrust is exerted across a liquid solvent suspended with bulk powder material. Nanosheets of graphene, TMDs, metal−organic frameworks (MOFs), and several other materials have been obtained via a liquid exfoliation route. Exfoliation results in high aspect ratio nanosheets with a high surface area, which necessarily turns advantageous for applications associated with the high surface area. A schematic illustration of the three types of liquid exfoliation is provided in Figure 5. The utmost prevailing method of synthesis of exfoliated layered crystals is oxidation. The use of a compatible

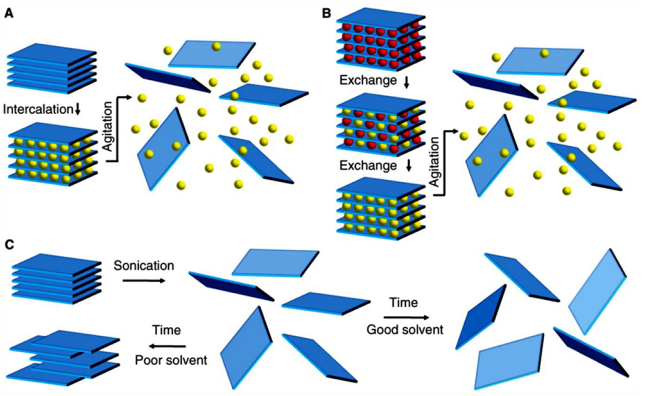

Figure 5. Schematic portrayal of the mechanisms in the three liquid exfoliation techniques. (A) Ion intercalation method where the ions (yellow spheres) are intercalated in between the layers. (B) Ion exchange where few layered compounds hold ions in between the layers, resulting in balancing the surface charge on the layers. In a liquid atmosphere, the ions (red spheres) can be replaced, often with bigger ions (yellow spheres). (C) Sonication-aided exfoliation where the crystal layered structures are sonicated in a solvent, causing exfoliation and nanosheet development. Reproduced with permission from ref 57. Copyright 2013, with permission from Science.

oxidizer results in the introduction of hydroxyl or epoxide functional groups in between the sheets, resulting in water intercalation and pronounced large-scale exfoliation upon ultrasonication. Use of a suitable stabilizer prevents reaggregation, and further reduction removes the oxides and introduces defects.[63] Synthesis of graphene in the form of reduced graphene oxide (rGO) is the best example of this kind of synthesis. Intercalation is another method that utilizes the space between the layered structures to introduce guest molecules, which helps in cleaving the sheets apart from their interlayer adhesive force.[63] Further sonication or thermal treatment results in complete exfoliation. Addition of surfactant supports the stabilization process. To synthesize several layers of graphene, Shih et al. introduced different types of halogen intercalates to introduce strain, which finally resulted in bi- or trilayered graphene sheets.[64] Xiong et al. studied the effects of lithium intercalation in between the interlayers of MoS_2.[65] The wide gap (0.615 nm) between this TMD provides space to host a wide range of molecules, which allows for further evaluation of the electronic and optical properties of the MoS_2 layers upon intercalation of Li ions.[66] However, this method does experience the drawback of being sensitive to ambient conditions.[67] Another approach in the liquid exfoliation technique is the ion exchange method.[68] This refers to the introduction of ionic charges opposite the charge of the layered sheets by replacing the existing ions to retain neutrality. The introduction of ions such as large organic molecules (e.g., quaternary ammonium cations, propylammonium cations, etc.) results in swelling, which eventually causes cleavage of the sheets.[69] Another, relatively easier technique is the application of ultrasonic waves in a solvent to introduce exfoliation of the layered materials. Studies illustrated the correct selection of solvent results in the stable synthesis of a bulk amount of 2D materials. The matching of the surface energy of the solvent and the layered materials contributes to the stability and reduces the possibility of reaggregation.[57]

Ternary metal carbides are a good example to illustrate liquid exfoliation. This class of layered solid structures have

DOI: 10.1021/acsenergylett.9b00940
ACS Energy Lett. 2019, 4, 1687−1709

strong bonds. Naguib et al. reported the synthesis of a range of 2D transition metal carbides and carbonitrides from their MAX phase in HF. Herein, MAX phase denotes the chemical composition $M_{n+1}AX_n$, where n = 1, 2, or 3, "M" represents an early transition metal, elements from group 13 and 14 represent the "A", and "X" is C and/or N. The A layers of the MAX phase are observed to be chemically more reactive as they are bonded weakly when compared to the M−X bonds. Different MAX phases were immersed in varying concentrations of HF for different intervals of time. The resultant powders were sonicated for different time intervals to yield layered structures of MXenes (Figure 6).[70]

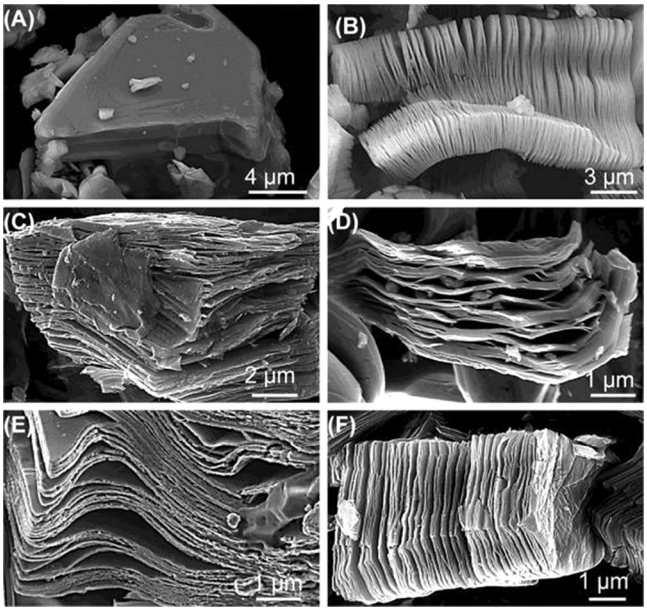

Figure 6. (A) Ti_3AlC_2 particle before treatment and after HF treatment of (B) Ti_3AlC_2, (C) Ti_2AlC, (D) Ta_4AlC_3, (E) TiNbAlC, and (F) Ti_3AlCN. Reproduced with permission from ref 70. Copyright 2012, American Chemical Society.

Similarly, the use of chemical exfoliation does cite some novel properties as they help in controlling the uniformity and the number of sheets by picking the correct solvent and exfoliation period. However, this method introduces intrinsic defects that require the construction of the monolayers as a post-treatment.

Solvothermal Synthesis. A chemical reaction of reactants in a sealed and heated pressurized atmosphere is defined as the solvothermal or hydrothermal synthesis. The use of water as a solvent for the reaction makes this process hydrothermal, while the use of any other solvent makes the reaction a solvothermal technique. The present synthesis process is different from solid-state reactions. In solid-state reactions, the mixing occurs at the interface, while in this case, the reaction occurs at the atomic scale in solution phase. Lowering of the reaction temperature and the ease in operability of this technique make it a lucrative option in synthesizing various categories of novel materials. In a recent book chapter, Feng et al. provided a very detailed understanding of the hydrothermal technique. The authors highlight the importance of solvent selection in the synthesis process. The density, surface tension, and viscosity are the vital parameters that decisively impact the kinetics of the reaction. This synthesis is performed using a high-pressure vessel known as an autoclave (Figure 7). These autoclaves or the hydrothermal reactors are suitable for performance under

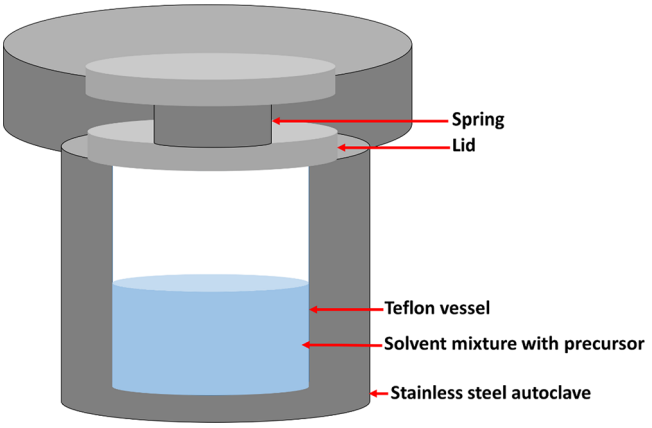

Figure 7. Schematic illustration of an autoclave vessel used for hydrothermal or solvothermal synthesis.

extreme temperature and pressure conditions. These vessels are resistant against acid, alkali, and other oxidants. They have a unique sealing feature that helps them retain heat and pressure for long-duration experiments. There have been numerous reports and a whole area dedicated to using this synthesis technique in NM synthesis. Reports of solvothermal or hydrothermal synthesis for 2D NMs and composites have also been widely reported.[71,72] The homogeneity of the NM and the control of the shape and size of the product make this process unique.[73]

In one such study, a CoP/BP heterostructure was prepared using ethanol as a solvent to dissolve all of the precursors of Co and P, which was further mixed with the BP nanosheets and subsequently treated at 160 °C for 3 h. The uniformly embedded CoP nanoparticles on the surface of the BP provide excellent interfacial contact, facilitating charge separation. The nanoparticles also prevent agglomeration of the sheets, which promotes retention of the high surface area and active sites of sheets. This benefits the photocatalytic hydrogen production.[74] In a recent study, a TiO_2@MoS_2 heterostructure was synthesized using hydrothermal synthesis. Titania nanobelts prepared using the simple hydrothermal procedure and acid corrosion techniques were directly added to the solution mixture of Mo and sulfur precursors. The suspension was thereafter treated at 200 °C for 24 h and further subjected to washing to attain the final product. The as-prepared samples exhibited high hydrogen production rates even in the absence of Pt and any sacrificial agent.[75] Similarly, Chava et al. utilized a two-step hydrothermal technique to develop a core−shell heteronanostructure. The CdS nanorods were prepared by a solvothermal technique (ethane diamine as a solvent) at 180 °C for 24 h. Additionally, the prepared CdS nanorods and Au nanoparticles were added along with the precursors of Mo and S to a suspension of DI water and further treated at 200 °C for 24 h. The obtained product was washed and dried to attain the final sample. The CdS-Au/MoS_2 nanostructure exhibited excellent H_2 evolution performance compared to their pure CdS nanorods. A Schottky junction is formed with the introduction of Au nanoparticles on CdS nanorods, which also promotes the formation of a core and shell of MoS_2 layers around it (Figure 8).[76]

DOI: 10.1021/acsenergylett.9b00940
ACS Energy Lett. 2019, 4, 1687−1709

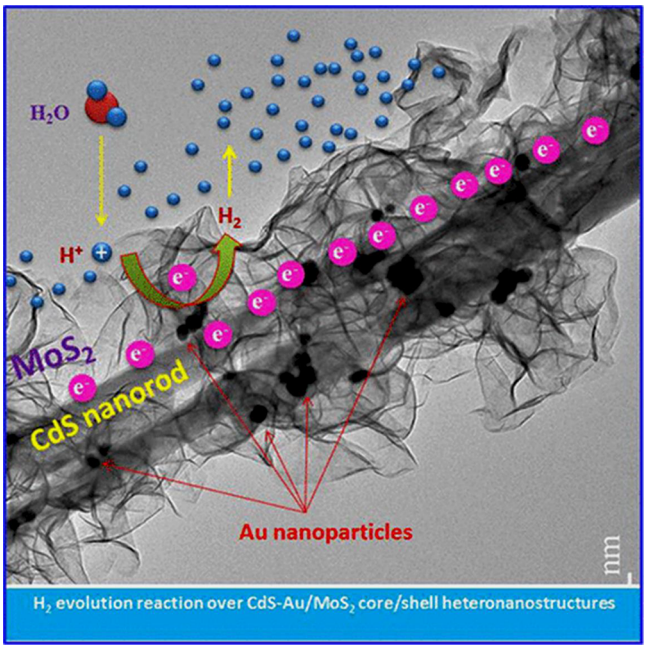

Figure 8. TEM image illustrating the formation of a 1D CdS-Au/MoS_2 hierarchical core/shell heteronanostructure that exhibits improved photocatalytic H_2 evolution. Reproduced with permission of ref 76. Copyright 2018, American Chemical Society.

In another report, the authors fabricated a Z-scheme nanostructure of 2D BP and $BiVO_4$. The BP nanoflakes were prepared by an ultrasonication exfoliation technique utilizing *N*-methyl-2-pyrrolidone (NMP) solution. The $BiVO_4$ nanosheets were synthesized using a hydrothermal process utilizing sodium dodecyl benzenesulfonate (SDBS) as a template. The electrostatic interaction between both 2D architectures promoted the charge separation and effectively contributed toward impressive H_2 production results in the absence of any sacrificial agent.[77] Wang et al. demonstrated the fabrication of novel 2D Bi_2MoO_6@Ag_2MoO_4 core−shell composites. The composite was prepared via a two-step hydrothermal technique. A definite amount of ammonium molybdate and bismuth nitrate with a mixture of ethanediol and water treated to 160 °C for 3 h helped in the formation of the Bi_2MoO_6 nanosheets. In the second step, adequate amounts of nanosheets were dispersed in polyvinylpyrrolidone (PVP) and silver acetate solution to obtain a composite structure. The sheet-like heterostructure helped in narrowing down the distance between the active sites and the charge carriers and also enhanced the number of active sites, which helped promote overall catalytic function.[78,79] Interestingly, solvothermal synthesis was utilized to synthesize graphitic carbon-layered TiO_2 hybrid architectures.[80] A definite amount of titanium(IV) isopropoxide and oleylamine was mixed with 1,2-ethanedithiol. Subsequently stirring for 1 h, the reaction mixture with precursor was moved to a Teflon-lined autoclave vessel for solvothermal synthesis at 200 °C for 24 h. After finishing, the black precipitate was washed with ethanol/hexane and later freeze-dried for a few days and finally dried in a tubular furnace at 200 °C for 24 h under Ar gas flow. The composite hybrid structure showed an excellent hydrogen evolution rate (3.046 mmol h^{-1} g^{-1}).[80] In another report, a pretreatment hydrothermal protocol was performed to attain a porous architecture of C_3N_4 sheets. Adding a thiourea solution with melamine with treatment at 180 °C for 20 h and then postcalcination at 520 °C for 3 h resulted in a porous architecture. The hydrogen production rate was enhanced 3.3 times compared to pristine C_3N_4 sheets. The defects introduced by the porous structure delayed the charge recombination and also increased the surface area.[81] Even though there have been many reports of synthesis of hybrid materials using the solvothermal technique, the control of sheet size and the uniformity of the structure are uncontrollable in this technique. Hence, more optimized synthesis protocols are still needed for uniform and controlled growth of 2D architectures at the bulk scale.

Chemical Vapor Deposition. This bottom-up synthesis technique is the parent of a family of processes. In this technique, a solid structure is deposited on a heated substrate from vapor by chemical reaction. Optimizing the substrate temperature, the type of substrate, the pressure of the inflow gas, and the mixture of gas determines the nature of the substrate formed (thin film, single crystal, or powder). The use of the CVD technique for the synthesis of high-surface-area 2D materials has been reported earlier. Reina et al. reported the synthesis of large-area films of graphene on the surface of a polycrystalline Ni film. Thermal annealing of the Ni surface prior to the CVD technique leads to the formation of flat terraces and steps similar to the single crystal, which minutely defines the layered growth of the graphene sheets.[82] The growth of a uniform layer of MoS_2 was initially attempted by basic sulfurization of the Mo thin layer.[83] In this process, the thin film retained the metallic nature; this was attributed to the presence of a small amount of unreacted Mo metal in the film. The direct reaction of the Mo metal predeposited on the surface controls the thickness of the final film. To overcome this limitation, synthesis of MoS_2 using MoO_3 and sulfur powder as reactants has been reported.[84] However, in several of the cases, the CVD technique yielded rod-like or nanoparticles of MoS_2.[85,86] Yet, in this technique, control of the predeposited metal oxide thin film is critical to obtain desired wafers. Another study reported the use of the atomic layer deposition technique.[87] The precise pulse mode enables the formation of accurate wide wafers. Nevertheless, in an alternative study, the authors utilized rGO as a pretreatment of the SiO_2/Si substrate.[88] The use of rGO helps in promoting the layered growth of the MoS_2 sheets.[89] 2D ultrathin $NiPS_3$ crystals were prepared on different substrates. The $Ni(OH)_2$ nanosheets developed on a different substrate and then were placed inside of a quartz tube and heated at 470 °C for 6 h in Ar gas. The few-atomic-layer crystals exhibited excellent photocatalytic properties in producing H_2 without using any sacrificial agent.[90] In a more recent report, the authors utilized CVD to deposit centimeter-sized ultrathin films of tantalum disulfide on an electrode material with gold foil. The hydrogen production efficiency was reported to be higher than that incorporating Pt as a co-catalyst.[91]

CVD is a reliable technique that achieves controlled and uniform growth of 2D nanoarchitectures. However, the use of precious metal substrates makes this process expensive and not convenient for bulk production.[92]

Electronic Structure Manipulation Strategy. There are different factors that affect the overall production of HER. The crucial factor lies in the high rate of electron−hole pair recombination. It is preferable to optimize the synthesis of catalysts that generate electron−hole pairs in the visible region. However, recombination occurs because of the short mean free paths of

DOI: 10.1021/acsenergylett.9b00940
ACS Energy Lett. 2019, 4, 1687−1709

It is preferable to optimize the synthesis of catalysts that generate electron−hole pairs in the visible region. However, recombination occurs because of the short mean free paths of the charge carriers and the deeper penetration of the irradiating photons.

the charge carriers and the deeper penetration of the irradiating photons. The charge carriers do not get enough time to reach the surface and participate in the photochemical reaction, which subsequently results in recombination.[93] As explained in a recent review done by Deng et al., it has been shown that the perturbation caused a uniform 2D arrangement of graphene-like structures, which readily modified the density of the states and effectively improved the catalytic function (Figure 9).[94]

Defect Engineering. Creating vacancy defects is a key structural engineering method to introduce shallow trap sites for the electrons. These result in migration of the photogenerated charge carriers and further contribute to reduction of the band gap of the material.[95−97] In an effort to increase the active sites on the surface of MoS_2, Xie et al. synthesized defect-rich ultrathin nanosheets of MoS_2. These nanosheets have the tendency to form cracks and smaller domains, resulting in the development of increased active sites.[98] Another study showed that the introduction of oxygen defects changed the MoS_2 phase to the octahedral metallic ones denoted as 1T-MoS_2. The new MoS_2 phase provides enhanced active sites, and the oxygen-incorporated defects accelerate the hydrogen evolution process.[99] Studies demonstrated the superior catalytic nature of the metallic MoS_2 (1T-MoS_2) compared to the semiconducting MoS_2 (2H-MoS_2) pahse.[24] The high electron mobility and the presence of increased active sites in basal planes and edges are considered prime reasons for the enhanced activity.[100] In one of such study, Maitra et al. demonstrated that highly nitrogenized graphene composites with 2H-MoS_2 behave as an electron channel, thereby enhancing the rate of hydrogen production, but it still remains lower than the output shown by single layers of 1T-MoS_2.[101]

As recently reported, the authors were able to introduce Zn vacancies on the surface of the ZnS on a composite with C_3N_4. The introduction of these vacancies helped in promoting the charge carriers and reducing the recombination rate. The close proximity of ZnS on the heterojunction with the C_3N_4 sheets helped stabilize the structure even after long photocatalytic use. These architectures showed 30 times enhanced rates (713.68 μmol h^{-1} g^{-1}) compared to those of pristine g-C_3N_4.[102] Pilarski et al. reported the fabrication of layered cesium titanate. The addition of a small percentage of copper into the vacancies resulted in a decrease of the overall band gap.[103] Zhang et al. illustrated the formation of defect-enriched sheets of C_3N_4. The controlled thermolysis of urea resulted in the introduction of defects at the edges of the sheets, which necessarily turned to be efficient sites for quenching the photogenerated holes. The porous structure exhibited improved hydrogen production activity (1917 μmol^{-1} g^{-1} h^{-1}) compared to its pristine counterpart.[27] In a more recent article, the authors engineered positioning of MoS_2 quantum dots at the S vacancies on the Zn facet of $ZnIn_2S_4$. These vacancies acted as an electron trap to restrict its transmission toward the Zn facet. Moreover, the quantum dots promoted quick migration of the electrons through the close Zn−S interface. Hence, the composite nanoheterostructure exhibited 11 times (6.884 mmol^{-1} g^{-1} h^{-1}) enhanced rates of hydrogen evolution output compared to bulk $ZnIn_2S_4$.[104]

As discussed in previous sections, the photocatalyst should efficiently benefit from the solar energy to stimulate electron−hole pairs, and the generated excitons are requested to be diffused on a short time scale to the surface of materials where the OER and HER reactions will take place. In contrast with bulk materials, 2D NMs have shorter paths for exciton diffusion. One common and typical example is the TMD monolayer, which does not even hold any "bulk" region. Hence, these materials possess good photoluminescence (PL) efficiency.[105−107] Besides, owing to their merits, such as direct and applicable band gap (i.e., ∼1.9 eV for the MoS_2 monolayer) and abundant resource elements (i.e., Mo or S), these materials attracted great attention in the (photo/

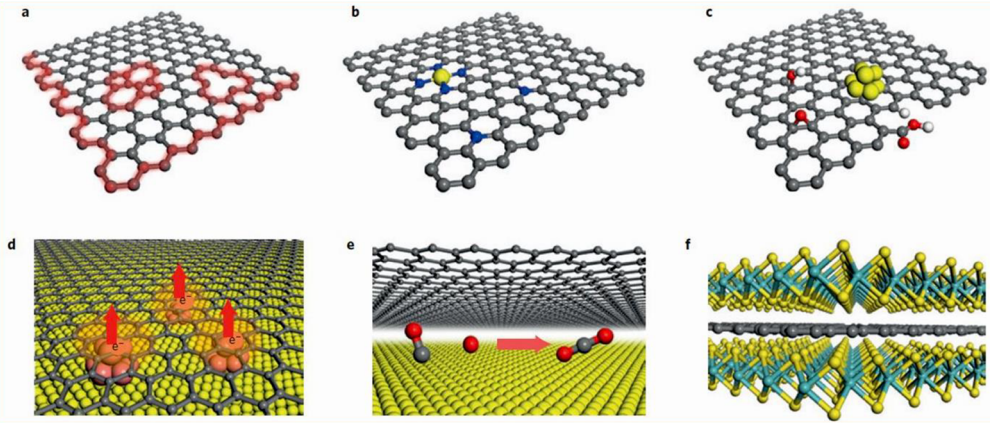

Figure 9. Schematic illustration of different graphene structures and their heterostructures with various catalytically active sites. (a) Formation of defects and edges. (b) Introduction of doped heteroatoms. (c) Functional groups and metal clusters. (d) Electron (e^-) movement from the metal to graphene layer results in improved activity. (e) Active site in between the spatial layer of the metal surface and 2D crystal. (f) Sandwich structure based on 2D materials observed in the case of graphene or MoS_2. Reproduced with permission from ref 94. Copyright 2016, with permission from Nature.

DOI: 10.1021/acsenergylett.9b00940
ACS Energy Lett. 2019, 4, 1687−1709

electro)catalytic fields immediately after they were successfully synthesized.[24,58,107−118]

However, there are still limitations regarding these kinds of materials. One critical problem relates to the fast annihilation of photogenerated excitons, which leads to a low QY.[119−122] Considering the fact that annihilation originates from the charge recombination between the electrons and holes, different strategies have been proposed to introduce additional energy barriers in order to enable enhancement of the charge separation and hinder the charge recombination. Following this, one main direction was focused on the synthesis of different types of heterojunctions consisting of two kinds of materials in the TMD family. For example, vertical heterojunctions[123,124] between two types of TMDs have been studied, and people found if a pair of excitons can stay at different layers, the lifetime of the exciton could be much longer. However, such a design might make the excitation process harder as well. Besides, considering the synthesis procedure, it was also hard to precisely control the relative orientations of two TMD monolayers, which may introduce additional complexity to the problem. Alternatively, the energy barrier may be introduced into one-layer heterojunctions, namely, the lateral or in-plane heterojunctions (LHJs).[125−130] It should be emphasized that the synthesis procedure is even harder compared with those for the synthesis of vertical heterojunctions, although almost all kinds of heterojunctions consisting of Mo, W, Se, and S were reported. Herein, we will present some discussions regarding this type of LHJ, especially for the defects at heterojunction interfaces.

It is very common to obtain some defects at the heterojunction interfaces, especially for those materials with relatively large lattice constant mismatch.[125−130] Taking the swap defect as one prototypical example, Cavallo's group fitted an empirical model based on DFT calculations.[131] The basic idea was analogous to the 2D Ising model, and they successfully decomposed the total energy into each pair of chemical bonds through the least-squares method, which can guarantee the global minimum of the solution. Employing this model, the W−S bonds revealed the strongest bonding energy, while the Mo−Se possessed the lowest bonding energy. This result led to the prediction that the WS_2−$MoSe_2$ LHJ may possess sharp interfaces at ideal conditions (or ∼0 K). However, under growing temperature (∼970 K), Monte Carlo simulations have given the result that this $MoSe_2$−WS_2 LHJ can still have abundant defects. This discovery highlighted the important role of the temperature (or entropy) effect from the thermodynamic route. It is worth mentioning that the performed Monte Carlo simulations did not consider the kinetic barriers of the material formation. It should be pointed out that with smart design employing the kinetic effects the number of defects may be reduced and materials quality thus improved.

Thereafter, Cavallo's group extended their discussions based on the materials with a relatively small number of defects at the interfacial region of the MoS_2−WSe_2 monolayer. Using a robust computational scheme, on the basis of DFT within the screened coulomb HSE06 exchange−correlation functional including the spin−orbit coupling, they validated their calculations by reproducing the experimental band gaps of MoS_2 and WSe_2 monolayers.[132133] Employing the same calculation algorithm, they extended the calculations to those LHJs formed by these two materials. The perfect LHJ revealed a narrower band gap (1.43 eV) than the band gaps of MoS_2 (2.07 eV) and WSe_2 (1.66 eV). Introducing interfacial swap defects, the band gaps were found to range from 1.42 to 1.55 eV. Interestingly, the band gap of the alloy-like monolayer introduced only a 0.13 eV band gap difference. Considering the precision of the DFT calculations, the difference is negligible, indicating that the defects may not affect the band gap of the LHJs that much.

Moreover, Cavallo's group aligned the conduction band minimum (CBM) of the pure materials and the LHJs with or without defects to the vacuum level.[131] As shown in Figure 10,

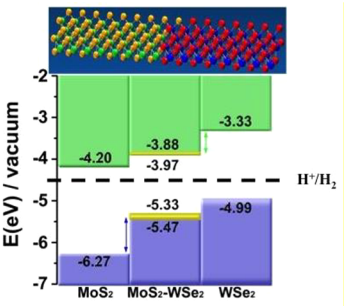

Figure 10. VBM and CBM energy alignment of the pure MoS_2 and WSe_2 monolayers as well as for their LHJs with representative types of defects using vacuum as a reference. The range of the calculated MoS_2−WSe_2 band gaps is indicated. Reprinted with permission from ref 131. Copyright 2017, American Chemical Society.

the WSe_2 monolayer revealed a higher CBM energy level than that obtained for the MoS_2 monolayer, leading to a type-II heterojunction. The CBM energy levels of the estimated LHJs were found to be located in between the pure MoS_2 and WSe_2 monolayers. The CBM energy levels observed for sharp and defective heterojunctions presented a slight difference (0.1−0.2 eV); however, it is not significant to alter the overall trend with CBM offsets in the 0.55−0.64 eV range. The energy band alignments of the pure monolayers before and after contact highlighted that the MoS_2−WSe_2 LHJ is an appreciable p−n junction, as observed in previously reported literature. Although both MoS_2 and WSe_2 monolayers revealed suitable CBM energy levels for HER with relative values of 0.3 and 1.17 eV higher than the H^+/H_2 potential, respectively, LHJs also showed suitable CBM energy positions located within a 0.53−0.62 eV range higher than the H^+/H_2 potential, highlighting another class of suitable materials for HER.[131]

Following the main idea related to the generation of additional energy barriers to enhance the charge separation and inhibit the charge recombination, they also focused on the kinetics study regarding the electrostatic potential (EP) generated by the LHJs. As shown in Figure 11, the perfect MoS_2−WSe_2 generated a sharp jump of EP profile at the interface, leading to the good driving force for exciton dissociation. The averaged EP profile of the heterojunction with a singular swap defect (as indicated by the red line in Figure 11) overlapped by that of the sharp interface (as indicated by the continuous black line) indicates that a partial number of defects would not decrease this driving force. On the other hand, the average EP profile for the alloy-like heterojunction showed a plateau wrapping the whole interface (Figure 11). This hump could decrease the driving energy for exciton dissociation, emphasizing the key advantage of interfaces with a restricted quantity of defects. Because of

DOI: 10.1021/acsenergylett.9b00940
ACS Energy Lett. 2019, 4, 1687−1709

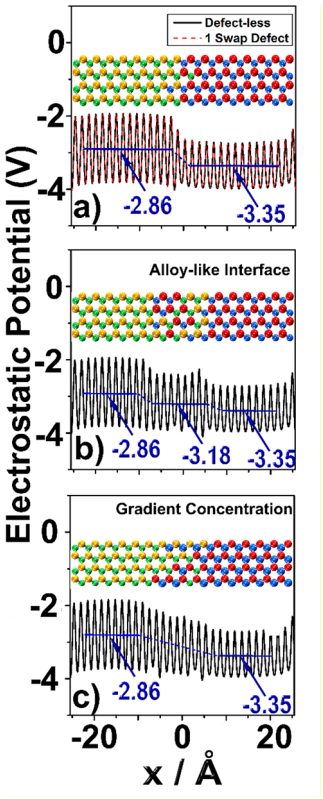

Figure 11. EP profile along the interface of the armchair MoS_2−WSe_2 LHJs with (a) sharp and one-swap defect interfaces, (b) an alloy-like interface, and (c) a gradient composition interface. Reprinted with permission from ref 131. Copyright 2017 American Chemical Society.

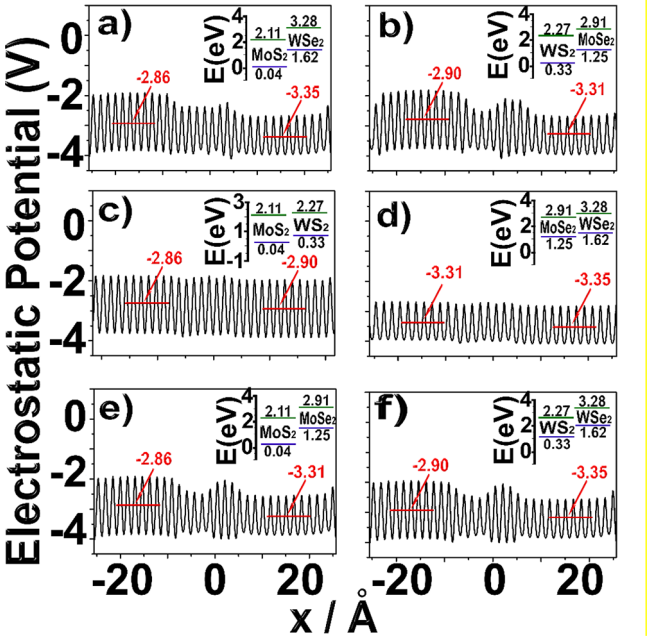

Figure 12. Self-consistent EP profile along the interface of the armchair LHJs for (a) MoS_2−WSe_2, (b) MoS_2−$MoSe_2$, (c) MoS_2−WS_2, (d) $MoSe_2$−WSe_2, (e) WS_2−WSe_2, and (f) $MoSe_2$−WS_2. Inset figures represent the band alignment based on the average EP of relaxed TMDs. For the sake of readability, the profile of MoS_2−WSe_2 is also reported together with the profile of the other TMDs. Reprinted with permission from ref 131. Copyright 2017 American Chemical Society.

the fact that added realistic interfaces might possess a gradient configuration that easily varies from MoS_2 to WSe_2, they also studied the EP profile in a typical system in which the interface was decreased to three MX_2 layers with % MoS_2/WSe_2 atom compositions of 75/25, 50/50, and 25/75 (random arrangement of the atoms). This structure resulted in an effortless variation in the EP profile after MoS_2 to WSe_2, validating the inference consequences by analyzing the alloy-like interface (Figure 11).

On the basis of this understanding, the Cavallo group also moved to studies regarding other LHJs consisting of Mo, S, W, and Se, leading to six types of LHJs (Figure 12).[131] Any combination consisting of two different materials within these four elements could generate type-II heterojunctions (or p−n junctions). This kind of electronic structure may be helpful to separate the electrons and holes into two materials. The only difference comes from the relative averaging EPs, which may determine the effect of charge separation. Similar to the MoS_2−WSe_2 LHJ, the WS_2−$MoSe_2$ also possessed a relatively large potential difference, indicating that the sharp LHJ can also be a good candidate for charge separation to provide a useful exciton. Both MoS_2−WS_2 and $MoSe_2$−WSe_2 showed a relatively smaller averaged potential energy difference, which requires better experimental skills to control the number of defects in the interfacial region. Defects in the rest of the LHJs could also induce relatively larger fluctuations, which might deteriorate the n−p-type performance.

In summary, the Cavallo group evaluated the impact on the stability and electronic properties of defects at the interface of monolayer LHJs through careful simulations.[131] The above strategy may be transferable to evaluate other materials. Comparison of sharp and defective MoS_2−WSe_2 LHJs allowed the authors to determine that redox and optoelectronic features, for example, the band gap and alignment together with the energy barrier to exciton dissociation/charge recombination, were slightly varied by the existence of a limited amount of defects and even through a ∼1 nm wide alloy-like interface. On the other hand, the defective interfacial region might compromise the capability of the material to endorse exciton dissociation, reducing quantum efficiency of most LHJs composed of Mo, W, S, and Se, emphasizing the relevance of establishing advanced protocols in synthesizing TMD LHJs with a minimal number of defects at the interfacial region.

Surface Engineering. Another approach to tune the physicochemical properties of the nanoarchitectures is surface engineering by surface modulation. This technique enables improvement of the band gap, electrical conductivity, and even magnetic properties of these 2D NMs. Tuning the nature of the exposed facet of the 2D NM by causing variation in the synthesis process shall determine the efficiency of the photocatalytic performance.[134] In one of the studies, the authors fabricated a heterostructure of GaN with MoS_2. The minute level of lattice mismatch helps in straddling the band alignment of the 2D sheets of the MoS_2 and 3D architecture of GaN. This necessarily helps in forming an indirect band gap with extensive visible-light absorption. The study details the impact of nitradation on the band gap alignment, which finds that enhanced hydrogen production results from the nitrated heterostructure.[135] Bie et al. reported the importance of

DOI: 10.1021/acsenergylett.9b00940
ACS Energy Lett. 2019, 4, 1687−1709

thickness of the layered structure (CdS) in the H_2 production efficiency. The authors found that a precise 3:5 ratio of sodium citrate and the Cd source resulted in the formation of 1.5 nm thick CdS nanosheets, which effectually illustrated three times enhanced output compared to CdS nanoparticles.[136] Nanosheets of $Zn_xCd_{1-x}S$ were prepared using ZnCdAl layered double hydroxides (LDHs) as a precursor and thiourea as a sulfur source (Figure 13). The nanosheets of these LDHs were

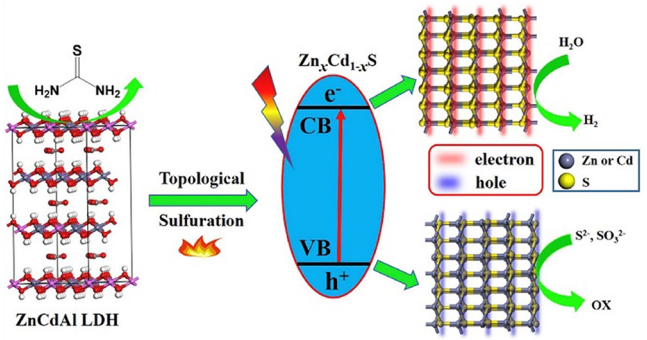

Figure 13. 2D ultrathin $Zn_xCd_{1-x}S$ nanosheets with exposed polar facet displaying enhanced H_2 production from water splitting. Reproduced with permission of ref 137 Copyright 2018, with permission from Elsevier.

attained by a topological sulfurization process, and fine-tuning of the precursor amount resulted in the formation of polar facets. The charge mobility along these facets was observed to be high, which effectively improved the H_2 generation ability.[137]

Yuan et al. reported the synthesis of $Ca_2Nb_3O_{10}$ and $Ti_{0.87}O_2$ nanosheets as a template for the growth of 2D oxide platelets with desired crystal orientation using a wet-chemical synthesis technique and calcination. These nanosheets displayed an impressive H_2 production efficiency.[138]

Employing the CVD method, TMDs could grow on different types of substrates, such as Al_2O_3, Si/SiO_2, or mica.[139] The lattice mismatch between the MoS_2 and substrate could bring severe troubles for the later applications of the produced TMDs due to the obtained grain boundaries.[140] Hence, people tried different strategies to minimize this effect and obtain large-size monolayer materials with good orientations of the seeds.[141,142]

Incorporation of Metal Nanoparticles. Apart from introducing structural defects, incorporation of metal nanoparticles on the semiconductor surface is certainly the easiest tailoring process to enhance the fundamental properties of the photocatalysts. This results in charge separation and accelerates the photochemical process. The enhancement of the band gap absorption in the visible region is attributed to the surface plasmon resonance (SPR) effect. The collective oscillation of the modes of CB electrons due to the electromagnetic interaction results in the overlap of the wave functions at the interface of the semiconductor/metal surface. This results in the formation of a depletion zone that causes bending in the band structure of the semiconductor. However, the charge transfer between the bands of the semiconductor surface and the metal surface depends on the band position of both materials. A Schottky barrier is developed in the interface to prevent the flow of charge carriers back to the semiconductor surface. In the case of n-type semiconductor materials, the electrons from the CB travel down to the metal surface and participate in the reduction process. On the other hand, the holes remain in their VB and participate in the oxidation process. In the case of a p-type semiconductor, the holes travel up to the metal surface while the electrons remain in the CB. However, the overall process is to halt the charge carriers from recombination, which eventually contributes to the hydrogen evolution process.

2D materials exhibit metastable states, in contrast to their traditional 3D bulk counterparts. Therefore, it is not that easy to obtain a single crystal of these materials. It should be noted that introducing metal clusters may induce unwanted phase transitions or additional boundaries.[143,144] This can lead to the destruction of the ideal single-phase TMDs, which is required in the applications. Hence, normal modification methods widely accepted in the 3D semiconductor materials should be redesigned before being employed in the TMD materials.

There are several reports highlighting the use of metal nanoparticles as potential co-catalysts to increase the visible-light absorption and contribute in the charge carrier separation interface. Hong et al. reported the synthesis of Cu-doped MoS_2 nanosheets on CdS nanorods. This ternary heterostructure was prepared in a two-step facile hydrothermal process. The composite nanostructure illustrated a 52-fold enhanced H_2 evolution output (194.18 μmol h^{-1} g^{-1}) compared to the pristine CdS nanorods. The synergistic effect of all three

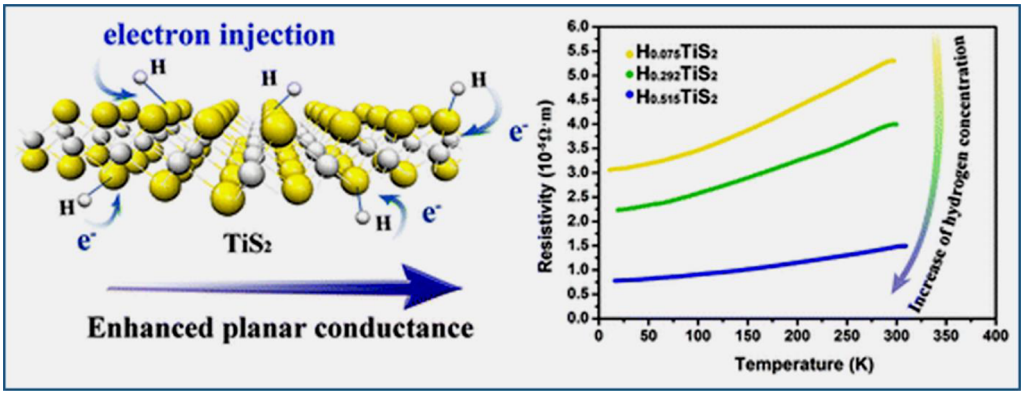

Figure 14. Graphical sketch highlighting the regulation of carrier concentration in metallic ultrathin TiS_2 by surface hydrogenation. Reproduced with permission from ref 147. Copyright 2013, American Chemical Society.

DOI: 10.1021/acsenergylett.9b00940
ACS Energy Lett. 2019, 4, 1687−1709

participants contributed to the overall enhancement of the materials performance.[145]

Incorporation of Nonmetal Heteroatoms. In one recent review article, Guo et al. summarized the impact of various chemical modifications on the physicochemical properties of 2D NMs.[146] The use of metal nanoparticles as co-catalysts has been widely reported, but these metals are often very rare and expensive for commercial-scale applications. Hence, finding other metal-free co-catalysts to serve the same goal is the primary focus. The incorporation of molecules or atoms on the surface of 2D NMs is to increase the electron migration, which effectively results in an increase of the intrinsic conductivity. In one such study, hydrogen at a precursor stage was added in the intermediate formation process, which resulted in hydrogen-added TiS_2 nanosheets (Figure 14). In this chemical reaction of H_yTiS_2, extra electrons were donated in between the sandwich layers of S−Ti−S layers. This led to superior electronic conductivity.[147] Apart from increasing the carrier concentrations, the surface modification via the introduction of molecules can control the carrier migration. The use of water molecules in VS_2 nanosheets resulted in an increase in the resistance. The carrier migrations (electrons) were observed from the V atoms present on the sides toward another nanosheet. Thus, the introduction of water molecules on the sides could effectively control the migration of the carriers and increase the resistance.[148] Similarly, oxygen was used as a potential dopant by controlling the crystallization process of MoS_2. The band gap of the ultrathin MoS_2 nanosheets was reduced compared to that of the undoped sample. The enhanced hybridization between the Mo-d orbital and S-p orbital resulted in reduction of the band gap. The oxygen atoms contributed to the charge density, which overall impacted the electronic structure of the material.[149]

Studies illustrating the use of atoms like sulfur and carbon as potential co-catalysts in a hybrid structure to enhance the photocatalytic activity of the composite have been conducted. A recent report detailed the fabrication of a 1D metallic MoO_2−C nanowire as a co-catalyst on a 2D C_3N_4 structure. The as-synthesized composite demonstrated approximately 150 times greater hydrogen production (1071.0 μmol h^{-1} g^{-1}) output compared to pristine 2D C_3N_4.[150] In a recent study, Li et al. reported a composite structure of $Mo_{15}S_{19}$ combined with CdS-diethylenetriamine (DETA). The hybrid structure reduced the overpotential of the H_2 evolution reaction and also improved the separation of photogenerated charge carriers.[151]

Recent Advances in Photocatalytic Hydrogen Evolution Reaction.

Transition Metal Dichalcogenide. TMDs have been an exciting class of layered materials. After a series of theoretical and experimental demonstrations, it was observed that the edges of S−Mo−S in the MoS_2 sheet are the active sites. Hence, multiple reports demonstrating strategies to enhance the number of active sites were reported. Fabrication of several nanoarchitectures like nanowires, nanorods, and nanosheets was aimed at improving the surface area of the structure.[58] The morphological alteration did not result in any changes in electronic property, but they eventually increased the number of active sites per unit area. In a recent study, the influence of a co-doped MoS_2/CdS composite for photocatalytic H_2 production was examined. Bare MoS_2 and CdS did not yield significant results owing to the fast recombination. On the other hand, doping at a certain wt % of MoS_2 resulted in enhancement of the yield (14.10 mmol h^{-1} g^{-1}). Combining the composite with Co resulted in enhanced H_2 production output.[152] Chen et al. reported the one-pot wet chemical fabrication of a CdS composite with a few-layer rich TMD (MoS_2 and WS_2). Few layers of TMDs grew upon the surface of CdS, and the nanohybrid between the two structures increased the number of surface active sites, which resulted in enhanced production output (WS_2−CdS 1984 mmol h^{-1} g^{-1} and MoS_2−CdS nanohybrids 1472 mmol h^{-1} g^{-1}).[153]

2D nanoplatelets or nanocrystals of Cd-based chalcogenides are interesting examples of chalcogenides compared to their bulk counterpart as their solar to H_2 conversion is relatively slow.[154−156] The high recombination rate plays a major role in this case because the platelet-like structures of the 2D crystals provide a larger cross section for light absorption and the strong confinement enables quick in-plane carrier transport.[157] Despite many advantageous properties, the charged excitons are extremely short-lived, prone to radiative and nonradiative recombination, which prevents their use as potential light harvesting centers. This problem is resolved by fabricating a type-II assembly of CdSe/CdTe core/crown heteronanosheets (with the CdTe crown laterally extending on the CdSe nanosheet core). The PL measurements suggested that the excitons were localized in domains, with electrons in CdSe and holes in CdTe. This exciton localization resulted in long-lived excitons and dampening of the recombination process.[158,159] Similarly, in another study, the authors explained the enhanced hydrogen production on Ni-decorated CdS nanorods. The semiconductor surface provides a site for a two-step mechanism for hole transfer employing the enhanced mobility of the $^{\bullet}OH/^{-}OH$ and its effective responses with the semiconductor and the sacrificial agent. This results in a high QY of H_2 generation.[160] In another study, the authors evaluated the H_2 generation efficiency of the CdSe capped with dihydrolipoic acid (DHLA) as the light absorber and a soluble Ni^{2+}-DHLA catalyst for proton reduction with ascorbic acid as an electron donor. The QY exhibited was more than 36%, and the durability of the material stood to be pretty impressive, making it an excellent candidate for water splitting systems.[161] Zhukovskyi and co-workers fabricated 2D CdS nanosheets of lateral dimension between 1 and 3 nm. Furthermore, Ni nanoparticles were photodeposited onto the nanosheets. The as-prepared materials were subjected to H_2 efficiency tests, which revealed an increase of 25% in AQY in Ni-decorated sheets compared to the pristine structures. The high efficiency obtained in the semiconductor/metal heterojunction is governed by the strong electron transfer.[162] Similarly, Xie et al. reported the formation of 2D sheets of NiOH/sulfide as a co-catalyst over CdS nanospheres. The sheets of nickel hydroxide and sulfide act as *hole* storage sites and surface reaction centers, which effectively promotes the charge transfer. This heterostructure combination pitches a 46 times higher evolution rate compared to CdS.[163]

Like chalcogenides, innovative 2D NMs, their synthesis, and hydrogen production efficiency have also recently received enhanced scientific attention.[164−166] The class of metal phosphorus trichalcogenide (MPX_3) requires low cleavage energy compared to graphite. The 2D quantum sheets (QSs) of $FePS_3$ are obtained from sonochemical exfoliation of the bulk in hydrazine solution.[167] The band gap of the material is 2.18 eV, significantly higher than that of bulk $FePS_3$ (1.6 eV). These 2D QSs of $FePS_3$ have exhibited an accelerated rate of

DOI: 10.1021/acsenergylett.9b00940
ACS Energy Lett. 2019, 4, 1687−1709

H_2 production (3 times the rate of bulk material), as shown in Figure 15.[167]

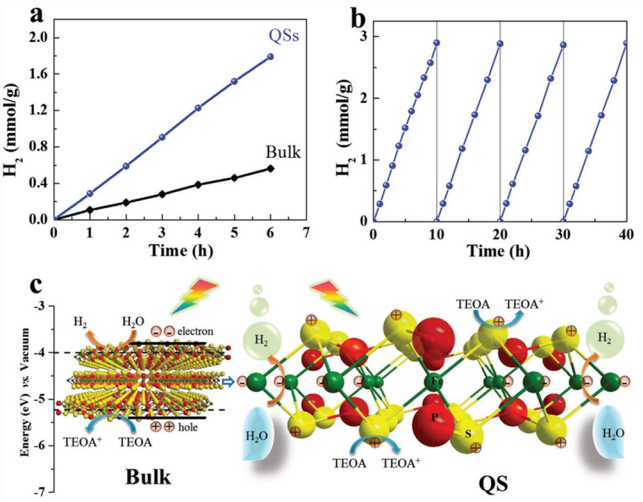

Figure 15. Schematic illustration of the photocatalytic activity of the bulk $FePS_3$ and QSs. (a) Photocatalytic H_2 generation plot of the bulk $FePS_3$ and QSs in 100 mL deionized water and 10% TEOA as a sacrificial agent. (b) Cycling measurements of H_2 generation of the $FePS_3$ QSs. (c) Graphical representation of photocatalytic processes for the bulk $FePS_3$ and QSs. Reproduced with permission from ref 167. Copyright 2018, with permission from Wiley.

MXenes and Novel Composites. A fascinating family of novel 2D NMs are transition metal carbides, nitrides, and carbonitrides, jointly mentioned as MXenes. MXenes have the general formula $M_{n+1}X_nT_x$ (n = 1−3), where M is a transition metal (such as Mo or Ti), X is C and/or N, and T_x symbolizes surface functional groups.[168,169] These layered 2D materials are derived from their parent layered, ternary carbides through careful etching of A group element atoms (Al/Ga/Si) in HF, NH_4HF_2, or LiF and HCl solutions.[177] These materials are strong, with better electrical conductivity and high electrical capacitance.[170−172] The presence of rich functional groups on the surface of MXenes makes them reliable candidates for doping with heteroatoms. Yuan et al. recently applied a novel method to fabricate a laminated defect-controlled carbon-supported sulfur-doped TiO_2 junction photocatalyst (LDC-S-TiO_2/C) including a sulfur impregnation procedure of Ti_3C_2. The authors found that the novel materials exhibited a high rate of H_2 generation (333 μmol h^{-1} g^{-1}). The novel synthesis process enabled increases in visible-light absorption, while theoretical analysis found that the activation energy required was also reduced. The synergistic effect contributed to the overall enhancement of the light-induced hydrogen generation.[173] Sun et al. reported the development of a composite of $Ti_3C_2T_x$ with carbon nitride. Usually, MXenes are metallic and hydrophilic in nature, but surface manipulation by introducing terminal oxygen results in a material with better catalytic properties. The as-prepared sample exhibited a 105% enhancement (88 μmol h^{-1} g^{-1}) in the H_2 production rate compared to the

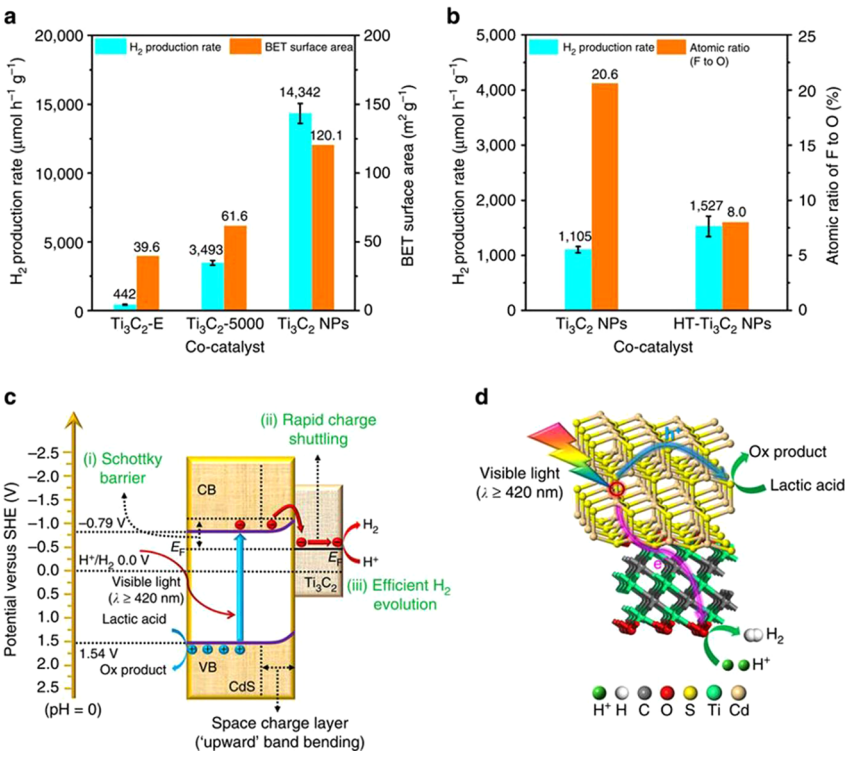

Figure 16. (a) Plot highlighting the effect of the surface area of the co-catalyst on the photocatalytic H_2 generation. (b) Plot highlighting the effect of the F to O atomic ratio on the surface of the co-catalyst on photocatalytic H_2 generation. (c) Schematic illustration of the charge separation and transfer occurring in the CdS/Ti_3C_2 upon visible-light illumination. The photogenerated electrons and holes are represented by red and blue spheres, respectively. (d) Plausible hydrogen generation mechanism in the CdS/Ti_3C_2 system upon visible-light irradiation. The green sphere denotes H^+. White, gray, red, yellow, cyan, and gold spheres denote H, C, O, S, Ti and Cd atoms, respectively. Reproduced with permission from ref 176. Copyright 2017, with permission from Nature.

DOI: 10.1021/acsenergylett.9b00940
ACS Energy Lett. 2019, 4, 1687−1709

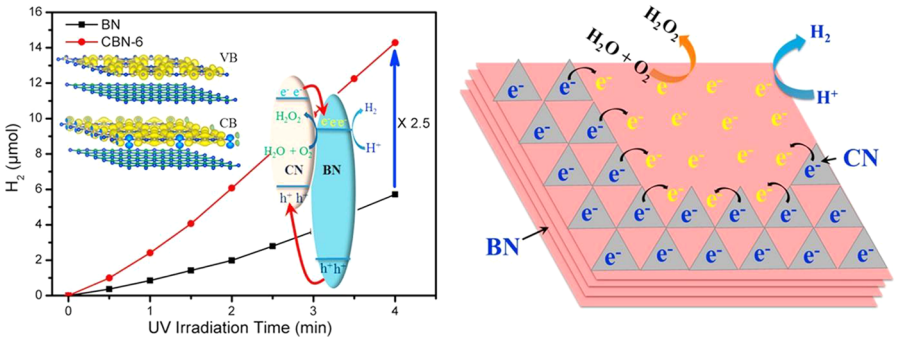

Figure 17. Photocatalytic mechanism illustrating the 2D heterojunction created by loading carbon nitride on h-BN nanosheets. Reproduced with permission from ref 183. Copyright 2017, with permission from Elsevier.

pristine samples.[174] In a recent report, Su and co-workers reported the development of a niobium pentoxide/carbon/niobium carbide hybrid photocatalyst. The MXene hybrid nanostructure exhibited a four times higher efficiency (7.81 μmol h^{-1} g^{-1}) than the pure niobium pentoxide. The enhanced efficiency was attributed to better charge separation in the interface, which in turn resulted in a lower rate of electron−hole recombination.[175] In another study, the authors fabricated a composite structure of CdS with Ti_3C_2 as an efficient co-catalyst. The composite exhibited 14 342 μmol h^{-1} g^{-1} of hydrogen evolution upon irradiation of photons at 420 nm (Figure 16).[176]

Peng et al. recently reported the fabrication of TiO_2 sheets (exposed on the (001) plane) grown on the surface of layered $Ti_3C_2T_x$ and later photodeposited nanodots of cuprous oxide on TiO_2. The functionalization of the basal plane of MXene results in it being a hole mediator, which tunnels electrons generated on the surface of TiO_2 and $Ti_3C_2T_x$ to travel to the nanodots (Cu_2O) to undergo reduction to elemental Cu. The Cu in the reaction process behaves like a potential reduction co-catalyst. The resultant photocatalyst demonstrates an efficiency of 860 μmol g^{-1} h^{-1} of hydrogen production.[178]

Graphene and Graphene-Like Materials. Wulan et al. recently reported the formation of nickel pyrophosphate-modified graphitic carbon nitride by a facile calcination technique and demonstrated the efficiency of the catalyst in photocatalytic water splitting. The as-synthesized catalyst demonstrated a 37 times enhanced rate of hydrogen production (207 μmol h^{-1} g^{-1}). The small particle size, good visible-light absorption, and fine reduction ability of the excited electrons contributed to the enhanced result.[179] Kong et al. reported a heterostructure of BP and g-C_3N_4. The BP served as a site for hole migration. The modified 2D structure exhibited an about 4 times enhanced H_2 production rate compared to pristine sheets of g-C_3N_4.[180] In a similar attempt, Meng et al. attempted a two-step thermal treatment on bulk sheets of carbon nitride to attain an atomically thin structure with high oxygen and amino groups. The formation of these groups provided rich active sites for surface reaction. The authors reported a drastic evolution rate of up to 20948.6 μmol h^{-1} g^{-1} using Pt as a co-catalyst.[181] Zeng et al. reported a novel heterojunction of 0D nickel phosphide-2D g-C_3N_4 sheets. A 3.5 wt % loading of Ni_2P nanoparticles was sufficient to achieve improved rates of hydrogen evolution. As described in several other reports, these novel interfaces are effective sites of the sink for excitons.[182] In another study, the authors fabricated a novel hybrid photocatalyst of carbon nitride and boron nitride (Figure 17). BN usually has a large band gap due to the wide VB. Loading of various amounts of carbon nitride resulted in band edge mismatch, which effectively contributed toward the charge separation. The overall output of the heterostructure was even better than that of Pt-loaded BN. Hence, this study demonstrated the basic fundamentals of band edge tuning to serve a catalytic purpose.[183]

Another study illustrated the incorporation of the 1,3,4,6,7,9,9*b*-heptaazaphenalene-2,5,8-triamine (melem) structure by destroying the polymeric structure of the carbon nitride by annealing treatment. This annealed structure exhibited wide absorption in the visible region. The annealed samples after further treatment with ammonia repaired the N vacancies and bridged the polymeric framework. These samples exhibited enhanced hydrogen production as they effectively harvest light and enable effective separation of the charge carriers.[184] Perovskite-based layered materials are an interesting class of materials. Their potential use as photocatalysts has recently taken more center stage in scientific research in hydrogen production. However, these layered structures have the disadvantage of low electron mobility. Nevertheless, these issues can be resolved by tuning them with a proper layered material like C_3N_4. $La_2Ti_2O_7$ nanosheets are hybridized with C_3N_4 sheets, where the C_3N_4 sheets act as a hole receptor and the perovskite nanosheets as an electron sink. This efficient interfacial charge transfer results in appreciable photocatalytic activity.[185] Chen et al. reported the synthesis of the g-C_3N_4/C_{60} hybrid structure obtained via mechanochemical route. Ball milling of fullerene in the presence of lithium hydroxide resulted in the formation of the hybrid structure. The authors debunked the use of any noble metals as potential co-catalysts and instead used the hybrid structure in bare conditions for visible-light-induced hydrogen production. The results illustrated an impressive increase in H_2 production up to 4 times compared to pristine g-C_3N_4 sheets.[186] Similarly, Lin et al. reported the synthesis of novel 2D/2D g-C_3N_4 nanosheet @$ZnIn_2S_4$ nanoleaf structures. The nanoheterojunction created channels for efficient charge separation, which resulted in an enhanced hydrogen production rate (2.78 mmol h^{-1} g^{-1}) compared to their pristine parent samples without using Pt as a co-catalyst.[187]

Metal−Organic Framework and Composites. MOFs are an interesting class of materials that have recently exhibited numerous applications in energy storage, and studies illustrating their photocatalytic behavior have been widely reported. The porous structure with high surface area and the ability to tailor the organic linkers or metal clusters make them an attractive class of materials to be considered for a wide range of applications. Hybrids with 2D NMs and other

DOI: 10.1021/acsenergylett.9b00940
ACS Energy Lett. 2019, 4, 1687−1709

inorganic materials for photocatalytic H_2 production are a domain worth exploring. Silva et al. were among the first to evaluate the photocatalytic behavior of UiO-66.[188] Irradiation of light with a wavelength greater than 300 nm in the presence of methanol as a sacrificial agent exhibited a high AQY.[188] In another study, the authors fabricated an amino-functionalized titanium(IV) MOF, where 2-amino-benzene dicarboxylic acid was used as an organic linker. Furthermore, Pt was photodeposited in the hybrid to be utilized in a H_2 production study. The aqueous solution contained triethanolamine as a sacrificial electron donor. The resulting hybrid materials showed interesting results; the organic linker motivated the light harvesting capability, and the excited electrons were transferred to the titanium−oxo clusters (Figure 18).[189]

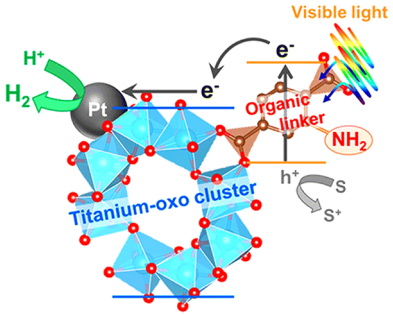

Figure 18. Schematic diagram illustrating the light-induced H_2 production in amino-functionalized titanium(IV) MOF. Reproduced with permission from ref 189. Copyright 2012, American Chemical Society.

Yan and co-workers fabricated a CdS-doped MOF (MIL-101) composite. The use of chalcogenide NMs for H_2 production has been reviewed in the earlier sections. The presence of compatible CB and VB edges makes chalcogenide interesting candidates, while the MOF provides enough room and surface sites for reaction time. The photodeposition of Pt over the composite was further evaluated for H_2 production. The 10 wt % loading of CdS showed the best result, and further runs up to 5 h showed excellent stability of the material.[190] In a similar attempt, Shen et al. studied the catalytic efficiency of metal (Au, Pd, and Pt) doped MOFs for H_2 production, using triethanolamine as a sacrificial agent. The results suggest that in the absence of Pt as a co-catalyst the output is very low compared to that of the doped materials. This shows the importance of co-catalysts and the use of sacrificial agent.[191] In an interesting study, Tilgner et al. fabricated a Au-doped anatase composite shell around a MOF core (MIL-101). Doping anatase TiO_2 with Au enhances the visible-light absorption. Using a MOF as a core provides strong structural stability as well as rendering enough surface sites to work around. The composite structure exhibits impressive production of 903 μmol h^{-1} g^{-1} of H_2 in a water/methanol solution.[192] In a very recent effort, Gao et al. studied the influence of $Co_xNi_{4-x}S_4$ on the surface of MIL-101 and studied the photocatalytic hydrogen production. The authors demonstrated the importance of surface atomic structures for fast electron transfer. The hydrogen generation process is initiated by H^+ adsorption, H^+ reduction, and the H_2 formation by further desorption. Hence, the adsorption arises to be the key step in the hydrogen evolution process, which determines the adsorption process and the driving force. Earlier reports suggest the difference in the activation energy aroused at different crystal facets due to the variation in the adsorption of the intermediate structure. Hence, studies evaluating structure orientation that provide low adsorption and overpotential energy are important. In this report, the authors observed that the dual transition metal sulfide ($Co_2Ni_2S_4$@MIL-101) exhibited the highest activity (Figure 19).[193]

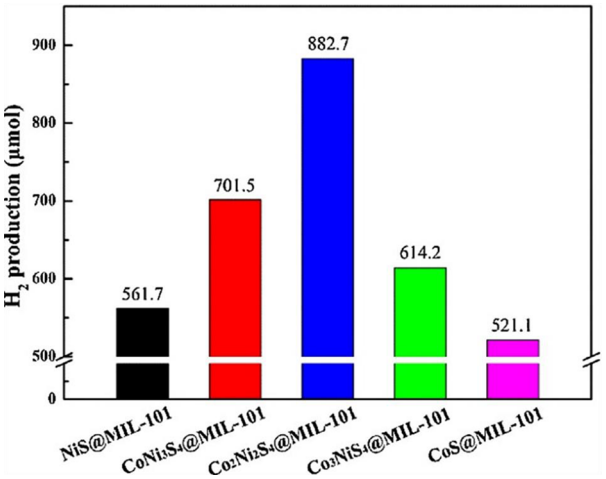

Figure 19. Hydrogen evolution over NiS@MIL-101, $CoNi_3S_4$@MIL-101, $Co_2Ni_2S_4$@MIL-101, Co_3NiS_4@MIL-101, and CoS@MIL-101 photocatalysts in 100 mL 10% (v/v) TEOA aqueous solution (pH 9) under visible-light irradiation ($\lambda \geq 420$ nm). Reproduced with permission from ref 193. Copyright 2017, with permission from Elsevier.

Novel Materials. In this section, recent studies on novel architectures and their photocatalytic behavior are detailed. 2D materials have always remained a thrust of interest compared to their bulk counterparts. Their ameliorable properties and a wide range of applicative domains make them interesting candidates for various energy and environmental applications. The 2D nanosheets provide the opportunity of less traveling for the incoming photon flux and increase the efficiency even in low intensity.[194] Reports of formation of p−n nanoheterojunctions have also appeared, which illustrates the importance of surface chemistry in building heterojunctions on the semiconductor surface.[195] Okamoto et al. studied the H_2 production efficiency of rhodium-doped calcium niobate nanosheets, fabricated by exfoliation of their pristine parent material. The 2D sheets exhibited an increase of 165-fold for the production efficiency compared to the parent material.[196] In another study, a novel heterojunction of $AgIn_5S_8/ZnIn_2S_4$ was fabricated. This 0D/2D heterojunction provided ample active sites as well as charge separation for the photogenerated charge carriers. The composite illustrated the maximum production rate (949.9 μmol h^{-1} g^{-1}) compared to their pristine parents.[197] Kong et al. reported the synthesis of plasma-engraved 2D TiO_2 (B) nanosheets. The plasma engraving resulted in the creation of oxygen vacancies, and these defects apparently reduced the overall band gap to 2.88 eV by introducing isolated bands. The hydrogen production output doubled the amount to 160 μmol h^{-1}.[198] Pilarski et al. synthesized layered cesium copper titanate structures and evaluated the structural efficiency of the material by hydrogen production study. The copper ions were deposited inside of the vacancies of cesium titanate and considerably enhanced the

DOI: 10.1021/acsenergylett.9b00940
ACS Energy Lett. 2019, 4, 1687−1709

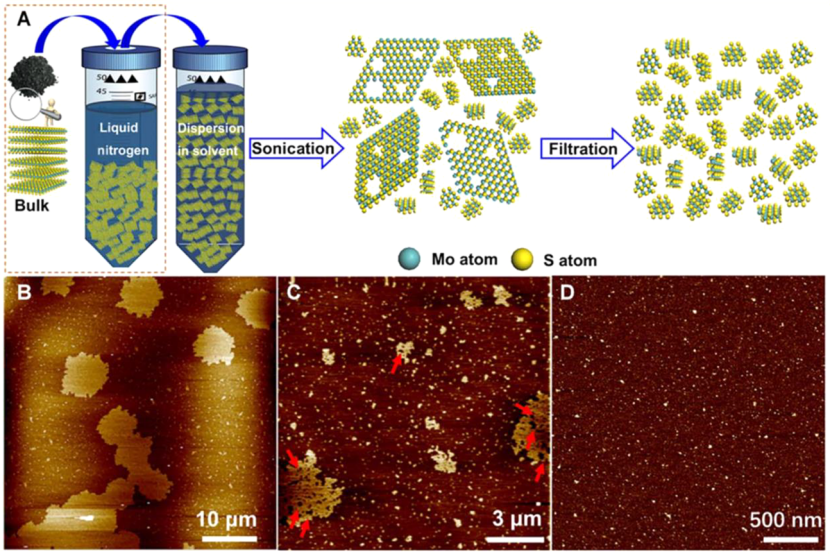

Figure 20. (A) Schematic display of the phases of preparation of 2D quantum dots. The highlighted section in a red rectangle represents the cryo pretreatment. (B–D) AFM results illustrating the formation of nanosheets to QDs, (B) ultrathin MoS_2 nanosheets at the delamination stage, (C) small MoS_2 nanosheets with tiny holes (the red arrows point to the holes), and (D) pure MoS_2 2D QDs after vacuum filtration. Reproduced with permission of ref 199. Copyright 2017, AAAS publishers.

visible-light absorption of the sample. The authors found a steady increase in the rate of H_2 production defined due to the copper atoms, which was reduced in the process into its metallic state and participated as a co-catalyst in the process.[103] In another set of interesting studies, Ajayan and co-workers demonstrated the formation of 2D quantum dots from exfoliated sheets of 2D NMs just by introducing a pretreatment in liquid N_2 for a definite time period (Figure 20). This process is a great leap in the existing strategies of LPEs as the cryo treatment necessarily brings about the process of getting pristine 2D structures predominantly as monolayers. The need for solvents specific for each exfoliation is not required anymore, and above all, use of any other impurities like surfactants is easily avoidable.[199]

Wen et al. reported the synthesis of a novel 2D core–shell nanostructure of $CuFeSe_2$@Au. The core formed is amorphous, and the shell is crystalline in nature. The unique architecture of the sample shows strong NIR absorption and illustrates an excellent H_2 evolution rate of 3.48 mmol h^{-1} g^{-1}.[200]

Prospects and Challenges. A great number of research advancements have been made by the scientific community in the past decade on utilizing solar power conversion to energy. In summary, the 2D NMs and their composite arrangements exhibit improved hydrogen production efficiency. The intimate interfaces result in delayed recombination pathways. Moreover, the charge carrier transport was enhanced by various fabrications or introduction of a secondary component such as a co-catalysts. The novel synthesis process of 2D/2D composite structures resulted in enhanced visible-light absorption and also improved the stability of the material against photocorrosion. Thus, these novel heterojunctions are a promising class of materials for future use. Regardless of the significant progress achieved in the past decade, there still remains a huge block of hurdles to cross with regards to photocatalytic water splitting reaction. Apart from materials synthesis and their core set of challenges, there lies another realm of concern related to hydrogen storage. It is indeed a critical issue of concern, which requires appropriate redress. The hydrogen with low volumetric energy can be compressed in the liquid or gas state, which requires high amounts of energy and would finally sum up in the cost of production. The problem of commercialization and the lack of technological support finally prevent consumers from purchasing hydrogen vehicles until an adequate supply of fuel is guaranteed. However, the idea of integrating a photocatalytic hydrogen generation unit with a storage entity can serve the realistic goals of solar to hydrogen energy utilization.[201] The formation of photogenerated charge carriers and the charge separation are extremely important with respect to attaining an efficient hydrogen production system. At present, the separation relies on the charge migration length, which is typically around 10–50 nm. As explained by Yang and co-workers, the protons generated in the oxidative sites are required to travel to the reductive sites of the material for hydrogen generation.[202] Subsequently, this leads to possible reverse reaction and contamination of hydrogen with oxygen. Thus, future research should primarily focus on effective electron transportation pathways to the oxidative sites. In the very same study, the author's proposed a multilayered structure of carbon nitride and graphene sheets. The theoretical estimation demonstrated that the light-generated holes migrate toward the exterior layers of graphene. The protons react with the inner electrons of the C_3N_4 sheets to form hydrogen. The H_2 generated is stored in between the sandwiched layers of graphene sheets as the selective absorption does not allow the passage of any other molecules.[202] In a similar effort, DFT studies also predict the use of porous BN for hydrogen storage and generation.[203] The formation of defects in h-BN results in a porous structure that enhances the specific surface area. Furthermore, doping with C results in a decrease in band gap from 3.98 to 1.8 eV. This curative architecture design of materials does necessarily define the upcoming innovative approach toward energy utilization. The use of 2D NMs like MXenes along with potential co-catalysts can also be worth designing for such a hybrid application. These heterojunction heterostructures have

DOI: 10.1021/acsenergylett.9b00940
ACS Energy Lett. 2019, 4, 1687–1709

The use of 2D NMs like MXenes along with potential co-catalysts can also be worth designing for such a hybrid application. These heterojunction heterostructures have illustrated significant efficiency compared to their singular components.

illustrated significant efficiency compared to their singular components. Mix and match of band structure alignment and utilizing the pros and cons of multiple components have resulted in better hydrogen production output. However, caution must prevail in the selection of materials for heterostructure, heterojunction composites. Understanding of the singular component is still relevant for rational design of the structure, such as the morphology, composition, interface engineering, etc.

On a critical note, even though there is an outpour of research publications, less have converted into productive commercialize technology. Publications communicating high production output of hydrogen often upon closer analysis reveal the presence of sacrificial electron donor or acceptors in the reaction.[204] Yet, on the bright side, the use of organic components as part of photoreforming and hydrogen generation has successfully led to different pilot-scale projects. In the same way, with respect to 2D materials, there lacks a complete understanding of the mechanism behind the catalytic activity. These materials are more often semiconducting in nature and exhibit poor charge transfer. Apart from that, the catalytically active sites are located at the edges or around the defects. The in-plane atoms remain catalytically inert in the process. Thus, 2D surfaces with appreciable charge kinetic ability are of paramount interest. Considerable numbers of studies at present are based on the trial-and-error stage and relate back to a first principle or DFT estimation. Synthesis of these materials has, to date, remained the single most challenging aspect for the whole scientific community. Therefore, the search for more efficient technologies for the bulk synthetic process is equally important. However, 2D materials and their composite architectures do exhibit promising features, but the careful rapport between theoretical and realistic approaches would finally convert them into useful technology. Hopefully, in the near future, the 2D material-based niche technologies will gradually pave from the laboratory benchtop experiment to industrial-scale applications.

Conclusions. In the past few years, photocatalytic water splitting has emerged as one of the most appropriate energy alternatives for future energy production. The rapid growth and interest exhibited by the scientific world have resulted in the fabrication of an interesting class of photoactive NMs. The major hurdle is the bulk synthesis of visible-light active photocatalysts with band structures suitable for the water splitting reaction. Recent fabrication strategies have resulted in novel nanostructures and their composites illustrating enhanced visible-light absorption and increased surface area. These architectures also displayed delayed charge recombination, which effectively enhanced the overall efficiency of the reaction. In this Review, we intended to provide a comprehensive discussion of the recent advances made in the field of photocatalytic hydrogen production by 2D materials. Apart from recent studies, a throwback of basic knowledge is detailed. The importance of electronic and band structure manipulations is highlighted. The different combination of synthesis techniques used for new 2D NMs is also described. Discussed are all of the apprehensions related to the technical advancements of this process. There remain multiple factors to address, and commercialization of this technology is one of such challenges for future research.

AUTHOR INFORMATION

Corresponding Authors

*E-mail: dionysdd@ucmail.uc.edu.
*E-mail: pillai.suresh@itsligo.ie.

ORCID

Priyanka Ganguly: 0000-0002-2709-2553
Moussab Harb: 0000-0001-5540-9792
Luigi Cavallo: 0000-0002-1398-338X
Suresh C. Pillai: 0000-0002-8901-9116

Notes

The authors declare no competing financial interest.

Biographies

Priyanka Ganguly is a Ph.D. candidate in the Nanotechnology and Bio-Engineering Research Group at the Institute of Technology Sligo, Ireland. She completed her M.Tech in Nanotechnology from Central University of Jharkhand, India. Her research interest lies in synthesis and characterization of 2D nanomaterials for energy and environmental applications including photocatalytic hydrogen production, antimicrobial disinfection, degradation, and toxicology.

Dr. Moussab Harb is currently a research scientist in computational solid-state physical chemistry at the KAUST Catalysis Center (KCC), Saudi Arabia. He obtained his Ph.D. in 2008 from the Light−Matter Institute (ILM) at the Claude Bernard University (UCBL), France. His research interests focus on designing new potential and efficient materials for solar-driven photocatalytic water splitting devices.

Dr. Zhen Cao completed his Ph.D. at the University of Chicago (USA) in 2015. Then, he moved to the King Abdullah University of Science and Technology (KAUST) as a postdoc at the KAUST Catalysis Center (KCC). He became a research scientist in the KCC from 2018.

Prof. Luigi Cavallo earned his Ph.D. in 1991 at the University of Naples, Italy, and completed his education on DFT working with Professor Tom Ziegler. In 2011, he joined the Catalysis Center at KAUST, Saudi Arabia, where her serves as Professor of Chemistry. His research interests focus on modeling heterogeneous and homogeneous catalysis.

Dr. Ailish Breen lectures Biopharmaceutical Science Engineering at the Institute of Technology Sligo, Ireland. She is a Biomedical Engineer with a Ph.D. in Biomedical Engineering from NUI Galway. Her research projects at present are investigating the potential of naturally derived polymers and manufacturing methods for controlled release of biomolecules and assessing the nanotoxicity of 2D materials.

Saoirse Dervin is a Ph.D. candidate in the Nanotechnology and Bio-Engineering research group at the Institute of Technology Sligo, Ireland. She graduated with a B.Sc. (Hons) in Forensic Investigation and Analysis from the Institute of Technology Sligo, Ireland. Her research interests include the synthesis, characteriation, and understanding of the mechanism of action of graphene and its functional derivatives for energy and environmental applications.

DOI: 10.1021/acsenergylett.9b00940
ACS Energy Lett. 2019, 4, 1687−1709

Prof. Dionysios (Dion) D. Dionysiou is currently a Professor of Environmental Engineering and Science and UNESCO CoChair Professor on "Water Access and Sustainability" at the University of Cincinnati. He teaches courses and performs research in the areas of drinking water quality and treatment, advanced oxidation technologies and nanotechnologies, and physical−chemical processes for water quality control.

Prof. Suresh C. Pillai is the head of the Nanotechnology and Bio-Engineering Research Group at the Institute of Technology Sligo, Ireland. He obtained his Ph.D. from Trinity College Dublin and completed postdoctoral research at Caltech, USA. His research interests include the synthesis of nanomaterials for energy and environmental applications.

■ ACKNOWLEDGMENTS

P.G. would like to thank the IT Sligo President's bursary for providing financial support. The authors would like to thank M.H., Z.C., and L.C. from King Abdullah University of Science and Technology (KAUST) for the computational contribution.

■ REFERENCES

(1) Furukawa, H.; Yaghi, O. M. Storage of hydrogen, methane, and carbon dioxide in highly porous covalent organic frameworks for clean energy applications. *J. Am. Chem. Soc.* **2009**, *131* (25), 8875−8883.
(2) Chalk, S. G.; Miller, J. F. Key challenges and recent progress in batteries, fuel cells, and hydrogen storage for clean energy systems. *J. Power Sources* **2006**, *159* (1), 73−80.
(3) Peschka, W. *Liquid hydrogen: fuel of the future*; Springer Science & Business Media: Springer, 2012.
(4) Li, Y.; Somorjai, G. A. Nanoscale advances in catalysis and energy applications. *Nano Lett.* **2010**, *10* (7), 2289−2295.
(5) Omer, A. M. Energy, environment and sustainable development. *Renewable Sustainable Energy Rev.* **2008**, *12* (9), 2265−2300.
(6) Chiesa, P.; Consonni, S.; Kreutz, T.; Williams, R. Co-production of hydrogen, electricity and CO_2 from coal with commercially ready technology. Part A: Performance and emissions. *Int. J. Hydrogen Energy* **2005**, *30* (7), 747−767.
(7) Rostrup-Nielsen, J. R.; Rostrup-Nielsen, T. Large-scale hydrogen production. *CATTECH* **2002**, *6* (4), 150−159.
(8) Gupta, U.; Rao, C. Hydrogen generation by water splitting using MoS_2 and other transition metal dichalcogenides. *Nano Energy* **2017**, *41*, 49−65.
(9) Teets, T. S.; Nocera, D. G. Photocatalytic hydrogen production. *Chem. Commun.* **2011**, *47* (33), 9268−9274.
(10) Kumaravel, V.; Mathew, S.; Bartlett, J.; Pillai, S. C. Photocatalytic hydrogen production using metal doped TiO_2: A review of recent advances. *Appl. Catal., B* **2019**, *244*, 1021−1064.
(11) Fujishima, A.; Honda, K. Electrochemical photolysis of water at a semiconductor electrode. *Nature* **1972**, *238*, 37−38.
(12) Grätzel, M. Photoelectrochemical cells. *Nature* **2001**, *414* (6861), 338.
(13) Wang, X.; Maeda, K.; Thomas, A.; Takanabe, K.; Xin, G.; Carlsson, J. M.; Domen, K.; Antonietti, M. A metal-free polymeric photocatalyst for hydrogen production from water under visible light. *Nat. Mater.* **2009**, *8* (1), 76−80.
(14) Zhou, X.; Liu, N.; Schmidt, J.; Kahnt, A.; Osvet, A.; Romeis, S.; Zolnhofer, E. M.; Marthala, V. R. R.; Guldi, D. M.; Peukert, W.; et al. Noble-Metal-Free Photocatalytic Hydrogen Evolution Activity: The Impact of Ball Milling Anatase Nanopowders with TiH_2. *Adv. Mater.* **2017**, *29* (5), 1604747.
(15) Ganguly, P.; Byrne, C.; Breen, A.; Pillai, S. C. Antimicrobial Activity of Photocatalysts: Fundamentals, Mechanisms, Kinetics and Recent Advances. *Appl. Catal., B* **2018**, *225*, 51−75.
(16) Ida, S.; Ishihara, T. Recent progress in two-dimensional oxide photocatalysts for water splitting. *J. Phys. Chem. Lett.* **2014**, *5* (15), 2533−2542.
(17) Novoselov, K.; Jiang, D.; Schedin, F.; Booth, T.; Khotkevich, V.; Morozov, S.; Geim, A. Two-dimensional atomic crystals. *Proc. Natl. Acad. Sci. U. S. A.* **2005**, *102* (30), 10451−10453.
(18) Castro Neto, A.; Novoselov, K. Two-Dimensional Crystals: Beyond Graphene. *Mat. Express* **2011**, *1* (1), 10−17.
(19) An, X.; Yu, J. Graphene-based photocatalytic composites. *RSC Adv.* **2011**, *1* (8), 1426−1434.
(20) Wei, Y.; Ma, Y.; Wei, W.; Li, M.; Huang, B.; Dai, Y. Promising Photocatalysts for Water Splitting in BeN_2 and MgN_2 Monolayers. *J. Phys. Chem. C* **2018**, *122* (15), 8102−8108.
(21) Makaremi, M.; Grixti, S.; Butler, K. T.; Ozin, G. A.; Singh, C. V. Band Engineering of Carbon Nitride Monolayers by N-Type, P-Type, and Isoelectronic Doping for Photocatalytic Applications. *ACS Appl. Mater. Interfaces* **2018**, *10* (13), 11143−11151.
(22) Xia, D. D.; Gong, F.; Pei, X.; Wang, W.; Li, H.; Zeng, W.; Wu, M.; Papavassiliou, D. V. Molybdenum and tungsten disulfides-based nanocomposite films for energy storage and conversion: A review. *Chem. Eng. J.* **2018**, *348*, 908−928.
(23) Coleman, J. N.; Lotya, M.; O'Neill, A.; Bergin, S. D.; King, P. J.; Khan, U.; Young, K.; Gaucher, A.; De, S.; Smith, R. J.; et al. Two-dimensional nanosheets produced by liquid exfoliation of layered materials. *Science* **2011**, *331* (6017), 568−571.
(24) Splendiani, A.; Sun, L.; Zhang, Y.; Li, T.; Kim, J.; Chim, C.-Y.; Galli, G.; Wang, F. Emerging photoluminescence in monolayer MoS_2. *Nano Lett.* **2010**, *10* (4), 1271−1275.
(25) Panneri, S.; Thomas, M.; Ganguly, P.; Nair, B. N.; Mohamed, A. P.; Warrier, K.; Hareesh, U. C_3N_4 anchored ZIF 8 composites: photo-regenerable, high capacity sorbents as adsorptive photocatalysts for the effective removal of tetracycline from water. *Catal. Sci. Technol.* **2017**, *7*, 2118−2128.
(26) Panneri, S.; Ganguly, P.; Mohan, M.; Nair, B. N.; Mohamed, A. A. P.; Warrier, K. G.; Hareesh, U. Photoregenerable, Bifunctional Granules of Carbon-Doped g-C3N4 as Adsorptive Photocatalyst for the Efficient Removal of Tetracycline Antibiotic. *ACS Sustainable Chem. Eng.* **2017**, *5* (2), 1610−1618.
(27) Zhang, Z.; Lu, L.; Lv, Z.; Chen, Y.; Jin, H.; Hou, S.; Qiu, L.; Duan, L.; Liu, J.; Dai, K. Porous carbon nitride with defect mediated interfacial oxidation for improving visible light photocatalytic hydrogen evolution. *Appl. Catal., B* **2018**, *232*, 384−390.
(28) Panneri, S.; Ganguly, P.; Nair, B. N.; Mohamed, A. A. P.; Warrier, K. G.; Hareesh, U. N. Copyrolysed C_3N_4-Ag/ZnO Ternary Heterostructure Systems for Enhanced Adsorption and Photocatalytic Degradation of Tetracycline. *Eur. J. Inorg. Chem.* **2016**, *2016* (31), 5068−5076.
(29) Panneri, S.; Ganguly, P.; Nair, B. N.; Mohamed, A. A. P.; Warrier, K. G. K.; Hareesh, U. N. S. Role of precursors on the photophysical properties of carbon nitride and its application for antibiotic degradation. *Environ. Sci. Pollut. Res.* **2017**, *24* (9), 8609−8618.
(30) Voiry, D.; Shin, H. S.; Loh, K. P.; Chhowalla, M. Low-dimensional catalysts for hydrogen evolution and CO_2 reduction. *Nature Reviews Chemistry* **2018**, *2*, 0105.
(31) Hu, W.; Yang, J. Two-dimensional van der Waals heterojunctions for functional materials and devices. *J. Mater. Chem. C* **2017**, *5* (47), 12289−12297.
(32) Cai, X.; Luo, Y.; Liu, B.; Cheng, H.-M. Preparation of 2D material dispersions and their applications. *Chem. Soc. Rev.* **2018**, *47*, 6224−6266.
(33) Kumar, P.; Boukherroub, R.; Shankar, K. Sunlight-driven water-splitting using two dimensional carbon based semiconductors. *J. Mater. Chem. A* **2018**, *6*, 12876−12931.
(34) Rosman, N. N.; Mohamad Yunus, R.; Jeffery Minggu, L.; Arifin, K.; Salehmin, M. N. I.; Mohamed, M. A.; Kassim, M. B. Photocatalytic properties of two-dimensional graphene and layered transition-metal dichalcogenides based photocatalyst for photoelectrochemical hydrogen generation: An overview. *Int. J. Hydrogen Energy* **2018**, *43*, 18925−18945.
(35) Xia, P.; Zhu, B.; Cheng, B.; Yu, J.; Xu, J. 2D/2D g-C_3N_4/MnO_2 nanocomposite as a direct Z-scheme photocatalyst for enhanced

DOI: 10.1021/acsenergylett.9b00940
ACS Energy Lett. 2019, 4, 1687−1709

photocatalytic activity. *ACS Sustainable Chem. Eng.* **2018**, *6* (1), 965−973.
(36) Su, T.; Shao, Q.; Qin, Z.; Guo, Z.; Wu, Z. Role of interfaces in two-dimensional photocatalyst for water splitting. *ACS Catal.* **2018**, *8* (3), 2253−2276.
(37) Luo, B.; Liu, G.; Wang, L. Recent advances in 2D materials for photocatalysis. *Nanoscale* **2016**, *8* (13), 6904−6920.
(38) Singh, A. K.; Mathew, K.; Zhuang, H. L.; Hennig, R. G. Computational screening of 2D materials for photocatalysis. *J. Phys. Chem. Lett.* **2015**, *6* (6), 1087−1098.
(39) Teoh, W.; Scott, J.; Amal, R. Progress in Heterogeneous Photocatalysis: From Classical Radical Chemistry to Engineering Nanomaterials and Solar Reactors. *J. Phys. Chem. Lett.* **2012**, *3* (5), 629−639.
(40) Parsons, R. The rate of electrolytic hydrogen evolution and the heat of adsorption of hydrogen. *Trans. Faraday Soc.* **1958**, *54*, 1053−1063.
(41) Hinnemann, B.; Moses, P. G.; Bonde, J.; Jørgensen, K. P.; Nielsen, J. H.; Horch, S.; Chorkendorff, I.; Nørskov, J. K. Biomimetic hydrogen evolution: MoS_2 nanoparticles as catalyst for hydrogen evolution. *J. Am. Chem. Soc.* **2005**, *127* (15), 5308−5309.
(42) Rao, C.; Dey, S. Solar thermochemical splitting of water to generate hydrogen. *Proc. Natl. Acad. Sci. U. S. A.* **2017**, *114* (51), 13385−13393.
(43) *Hydrogen Production: Thermochemical Water Splitting*. https://www.energy.gov/eere/fuelcells/hydrogen-production-thermochemical-water-splitting (accessed May 6, 2019).
(44) Wu, X.; Onuki, K. Thermochemical water splitting for hydrogen production utilizing nuclear heat from an HTGR. *Tsinghua Sci. Technol.* **2005**, *10* (2), 270−276.
(45) Das, D.; Veziroğlu, T. N. Hydrogen production by biological processes: a survey of literature. *Int. J. Hydrogen Energy* **2001**, *26* (1), 13−28.
(46) Maness, P.-C.; Yu, J.; Eckert, C.; Ghirardi, M. L. Photobiological hydrogen production−prospects and challenges. *Microbe* **2009**, *4* (6), 659−667.
(47) Poudyal, R.; Tiwari, I.; Koirala, A.; Masukawa, H.; Inoue, K.; Tomo, T.; Najafpour, M.; Allakhverdiev, S.; Veziroğlu, T., Hydrogen production using photobiological methods. *Compendium of Hydrogen Energy*; Elsevier, 2015; pp 289−317.
(48) Asada, Y.; Miyake, J. Photobiological hydrogen production. *J. Biosci. Bioeng.* **1999**, *88* (1), 1−6.
(49) Fujishima, A.; Honda, K. Electrochemical photolysis of water at a semiconductor electrode. *Nature* **1972**, *238* (5358), 37−38.
(50) Bard, A. J. Photoelectrochemistry and heterogeneous photocatalysis at semiconductors. *J. Photochem.* **1979**, *10* (1), 59−75.
(51) Xie, G.; Zhang, K.; Guo, B.; Liu, Q.; Fang, L.; Gong, J. R. Graphene-based materials for hydrogen generation from light-driven water splitting. *Adv. Mater.* **2013**, *25* (28), 3820−3839.
(52) Ren, Y.; Xu, Q.; Zheng, X.; Fu, Y.; Wang, Z.; Chen, H.; Weng, Y.; Zhou, Y. Building of peculiar heterostructure of Ag/two-dimensional fullerene shell-WO_{3-x} for enhanced photoelectrochemical performance. *Appl. Catal., B* **2018**, *231*, 381−390.
(53) Li, X.; Yu, J.; Low, J.; Fang, Y.; Xiao, J.; Chen, X. Engineering heterogeneous semiconductors for solar water splitting. *J. Mater. Chem. A* **2015**, *3* (6), 2485−2534.
(54) Devaraji, P.; Jo, W. K. Two-dimensional Mixed Phase Leaf-$Ti_{1-x}Cu_xO_2$ Sheets Synthesized Based on a Natural Leaf Template for Increased Photocatalytic H_2 Evolution. *ChemCatChem* **2018**, *10* (17), 3813−3823.
(55) Wang, C.; Lv, P.; Xue, D.; Cai, Y.; Yan, X.; Xu, L.; Fang, J.; Yang, Y. Zero-Dimensional/Two-Dimensional Au25 (Cys)18 Nanoclusters/g-C_3N_4 Nanosheets Composites for Enhanced Photocatalytic Hydrogen Production under Visible Light. *ACS Sustainable Chem. Eng.* **2018**, *6* (7), 8447−8457.
(56) Peng, J.; Wu, J.; Li, X.; Zhou, Y.; Yu, Z.; Guo, Y.; Wu, J.; Lin, Y.; Li, Z.; Wu, X.; et al. Very large-sized transition metal dichalcogenides monolayers from fast exfoliation by manual shaking. *J. Am. Chem. Soc.* **2017**, *139* (26), 9019−9025.
(57) Nicolosi, V.; Chhowalla, M.; Kanatzidis, M.; Strano, M.; Coleman, J. Liquid Exfoliation of Layered Materials. *Science* **2013**, *340* (6139), 1420.
(58) Mak, K. F.; Lee, C.; Hone, J.; Shan, J.; Heinz, T. F. Atomically thin MoS 2: a new direct-gap semiconductor. *Phys. Rev. Lett.* **2010**, *105* (13), 136805.
(59) Hong, S. S.; Kundhikanjana, W.; Cha, J. J.; Lai, K.; Kong, D.; Meister, S.; Kelly, M. A.; Shen, Z.-X.; Cui, Y. Ultrathin topological insulator Bi_2Se_3 nanoribbons exfoliated by atomic force microscopy. *Nano Lett.* **2010**, *10* (8), 3118−3122.
(60) Radisavljevic, B.; Radenovic, A.; Brivio, J.; Giacometti, i. V.; Kis, A. Single-layer MoS 2 transistors. *Nat. Nanotechnol.* **2011**, *6* (3), 147.
(61) Castellanos-Gomez, A.; Vicarelli, L.; Prada, E.; Island, J. O.; Narasimha-Acharya, K.; Blanter, S. I.; Groenendijk, D. J.; Buscema, M.; Steele, G. A.; Alvarez, J.; et al. Isolation and characterization of few-layer black phosphorus. *2D Materials* **2014**, *1* (2), 025001.
(62) Huang, Y.; Sutter, E.; Shi, N. N.; Zheng, J.; Yang, T.; Englund, D.; Gao, H.-J.; Sutter, P. Reliable exfoliation of large-area high-quality flakes of graphene and other two-dimensional materials. *ACS Nano* **2015**, *9* (11), 10612−10620.
(63) Eda, G.; Yamaguchi, H.; Voiry, D.; Fujita, T.; Chen, M.; Chhowalla, M. Photoluminescence from Chemically Exfoliated MoS_2. *Nano Lett.* **2011**, *11* (12), 5111−5116.
(64) Shih, C.; Vijayaraghavan, A.; Krishnan, R.; Sharma, R.; Han, J.; Ham, M.; Jin, Z.; Lin, S.; Paulus, G.; Reuel, N.; Wang, Q.; Blankschtein, D.; Strano, M. Bi- and trilayer graphene solutions. *Nat. Nanotechnol.* **2011**, *6* (7), 439−445.
(65) Xiong, F.; Wang, H.; Liu, X.; Sun, J.; Brongersma, M.; Pop, E.; Cui, Y. Li Intercalation in MoS2: In Situ Observation of Its Dynamics and Tuning Optical and Electrical Properties. *Nano Lett.* **2015**, *15* (10), 6777−6784.
(66) Rasamani, K.; Alimohammadi, F.; Sun, Y. Interlayer-expanded MoS_2. *Mater. Today* **2017**, *20* (2), 83−91.
(67) Kang, J.; Ke, M.; Hu, Y. Ionic Intercalation in Two-Dimensional van der Waals Materials: In Situ Characterization and Electrochemical Control of the Anisotropic Thermal Conductivity of Black Phosphorus. *Nano Lett.* **2017**, *17* (3), 1431−1438.
(68) Kim, T.; Lee, H.; Kim, J.; Suh, K. S. Synthesis of phase transferable graphene sheets using ionic liquid polymers. *ACS Nano* **2010**, *4* (3), 1612−1618.
(69) Ma, R.; Sasaki, T. Nanosheets of oxides and hydroxides: Ultimate 2D charge-bearing functional crystallites. *Adv. Mater.* **2010**, *22* (45), 5082−5104.
(70) Naguib, M.; Mashtalir, O.; Carle, J.; Presser, V.; Lu, J.; Hultman, L.; Gogotsi, Y.; Barsoum, M. Two-Dimensional Transition Metal Carbides. *ACS Nano* **2012**, *6* (2), 1322−1331.
(71) Han, C.; Zhang, Y.; Gao, P.; Chen, S.; Liu, X.; Mi, Y.; Zhang, J.; Ma, Y.; Jiang, W.; Chang, J. High-Yield Production of MoS_2 and WS_2 Quantum Sheets from Their Bulk Materials. *Nano Lett.* **2017**, *17* (12), 7767−7772.
(72) Yu, H.; Huang, H.; Xu, K.; Hao, W.; Guo, Y.; Wang, S.; Shen, X.; Pan, S.; Zhang, Y. Liquid-Phase Exfoliation into Monolayered BiOBr Nanosheets for Photocatalytic Oxidation and Reduction. *ACS Sustainable Chem. Eng.* **2017**, *5* (11), 10499−10508.
(73) Feng, S.-H.; Li, G.-H., Hydrothermal and solvothermal syntheses. *Modern Inorganic Synthetic Chemistry* 2nd ed.; Elsevier, 2017; pp 73−104.
(74) Liang, Q.; Shi, F.; Xiao, X.; Wu, X.; Huang, K.; Feng, S. In Situ Growth of CoP Nanoparticles Anchored on Black Phosphorus Nanosheets for Enhanced Photocatalytic Hydrogen Production. *ChemCatChem* **2018**, *10* (10), 2179−2183.
(75) Zhou, W.; Yin, Z.; Du, Y.; Huang, X.; Zeng, Z.; Fan, Z.; Liu, H.; Wang, J.; Zhang, H. Synthesis of Few-Layer MoS_2 Nanosheet-Coated TiO_2 Nanobelt Heterostructures for Enhanced Photocatalytic Activities. *Small* **2013**, *9* (1), 140−147.
(76) Chava, R.; Do, J.; Kang, M. Smart Hybridization of Au Coupled CdS Nanorods with Few Layered MoS_2 Nanosheets for High Performance Photocatalytic Hydrogen Evolution Reaction. *ACS Sustainable Chem. Eng.* **2018**, *6* (5), 6445−6457.

DOI: 10.1021/acsenergylett.9b00940
ACS Energy Lett. 2019, 4, 1687−1709

(77) Zhu, M.; Sun, Z.; Fujitsuka, M.; Majima, T. Z-Scheme Photocatalytic Water Splitting on a 2D Heterostructure of Black Phosphorus/Bismuth Vanadate Using Visible Light. *Angew. Chem., Int. Ed.* **2018**, *57* (8), 2160−2164.
(78) Wang, Z.; Huo, Y.; Zhang, J.; Lu, C.; Dai, K.; Liang, C.; Zhu, G. Facile preparation of two-dimensional Bi_2MoO_6@Ag_2MoO_4 core-shell composite with enhanced visible light photocatalytic activity. *J. Alloys Compd.* **2017**, *729*, 100−108.
(79) Feng, W.; Wang, Y.; Huang, X.; Wang, K.; Gao, F.; Zhao, Y.; Wang, B.; Zhang, L.; Liu, P. One-pot construction of 1D/2D $Zn_{1-x}Cd_xS$/D-$ZnS_{(en)(0.5)}$ composites with perfect heterojunctions and their superior visible-light-driven photocatalytic H_2 evolution. *Appl. Catal., B* **2018**, *220*, 324−336.
(80) Wang, S.; Li, J.; Wang, S.; Wu, J.; Wong, T.; Foo, M.; Chen, W.; Wu, K.; Xu, G. Two-Dimensional C/TiO2 Heterogeneous Hybrid for Noble-Metal-Free Hydrogen Evolution. *ACS Catal.* **2017**, *7* (10), 6892−6900.
(81) Huang, H.; Xiao, K.; Tian, N.; Dong, F.; Zhang, T.; Du, X.; Zhang, Y. Template-free precursor-surface-etching route to porous, thin gC_3N_4 nanosheets for enhancing photocatalytic reduction and oxidation activity. *J. Mater. Chem. A* **2017**, *5* (33), 17452−17463.
(82) Reina, A.; Jia, X.; Ho, J.; Nezich, D.; Son, H.; Bulovic, V.; Dresselhaus, M. S.; Kong, J. Large area, few-layer graphene films on arbitrary substrates by chemical vapor deposition. *Nano Lett.* **2009**, *9* (1), 30−35.
(83) Zhan, Y.; Liu, Z.; Najmaei, S.; Ajayan, P. M.; Lou, J. Large-area vapor-phase growth and characterization of MoS2 atomic layers on a SiO_2 substrate. *Small* **2012**, *8* (7), 966−971.
(84) Lin, Y.-C.; Zhang, W.; Huang, J.-K.; Liu, K.-K.; Lee, Y.-H.; Liang, C.-T.; Chu, C.-W.; Li, L.-J. Wafer-scale MoS_2 thin layers prepared by MoO_3 sulfurization. *Nanoscale* **2012**, *4* (20), 6637−6641.
(85) Li, X. L.; Li, Y. D. Formation of MoS_2 inorganic fullerenes (IFs) by the reaction of MoO_3 nanobelts and S. *Chem. - Eur. J.* **2003**, *9* (12), 2726−2731.
(86) Balendhran, S.; Ou, J. Z.; Bhaskaran, M.; Sriram, S.; Ippolito, S.; Vasic, Z.; Kats, E.; Bhargava, S.; Zhuiykov, S.; Kalantar-Zadeh, K.; et al. Nanoscale 4, 461 (2012). *Nanoscale* **2012**, *4*, 461.
(87) Song, J.-G.; Park, J.; Lee, W.; Choi, T.; Jung, H.; Lee, C. W.; Hwang, S.-H.; Myoung, J. M.; Jung, J.-H.; Kim, S.-H.; et al. Layer-controlled, wafer-scale, and conformal synthesis of tungsten disulfide nanosheets using atomic layer deposition. *ACS Nano* **2013**, *7* (12), 11333−11340.
(88) Pacley, S.; Hu, J.; Jespersen, M.; Hilton, A.; Waite, A.; Brausch, J.; Beck-Millerton, E.; Voevodin, A. A. Impact of reduced graphene oxide on MoS_2 grown by sulfurization of sputtered MoO_3 and Mo precursor films. *J. Vac. Sci. Technol., A* **2016**, *34* (4), 041505.
(89) Lee, Y. H.; Zhang, X. Q.; Zhang, W.; Chang, M. T.; Lin, C. T.; Chang, K. D.; Yu, Y. C.; Wang, J. T. W.; Chang, C. S.; Li, L. J.; et al. Synthesis of large-area MoS_2 atomic layers with chemical vapor deposition. *Adv. Mater.* **2012**, *24* (17), 2320−2325.
(90) Wang, F.; Shifa, T.; He, P.; Cheng, Z.; Chu, J.; Liu, Y.; Wang, Z.; Wang, F.; Wen, Y.; Liang, L.; He, J. Two-dimensional metal phosphorus trisulfide nanosheet with solar hydrogen-evolving activity. *Nano Energy* **2017**, *40*, 673−680.
(91) Shi, J.; Wang, X.; Zhang, S.; Xiao, L.; Huan, Y.; Gong, Y.; Zhang, Z.; Li, Y.; Zhou, X.; Hong, M.; et al. Two-dimensional metallic tantalum disulfide as a hydrogen evolution catalyst. *Nat. Commun.* **2017**, *8* (1), 958.
(92) Shi, Y.; Li, H.; Li, L.-J. Recent advances in controlled synthesis of two-dimensional transition metal dichalcogenides via vapour deposition techniques. *Chem. Soc. Rev.* **2015**, *44* (9), 2744−2756.
(93) Gomathi Devi, L.; Kavitha, R. A review on plasmonic metal-TiO_2 composite for generation, trapping, storing and dynamic vectorial transfer of photogenerated electrons across the Schottky junction in a photocatalytic system. *Appl. Surf. Sci.* **2016**, *360*, 601−622.
(94) Deng, D.; Novoselov, K.; Fu, Q.; Zheng, N.; Tian, Z.; Bao, X. Catalysis with two-dimensional materials and their heterostructures. *Nat. Nanotechnol.* **2016**, *11* (3), 218−230.
(95) Zheng, Y.; Jiao, Y.; Jaroniec, M.; Qiao, S. Advancing the Electrochemistry of the Hydrogen-Evolution Reaction through Combining Experiment and Theory. *Angew. Chem., Int. Ed.* **2015**, *54* (1), 52−65.
(96) Shu, H.; Zhou, D.; Li, F.; Cao, D.; Chen, X. Defect Engineering in MoSe2 for the Hydrogen Evolution Reaction: From Point Defects to Edges. *ACS Appl. Mater. Interfaces* **2017**, *9* (49), 42688−42698.
(97) Hu, W.; Lin, L.; Zhang, R.; Yang, C.; Yang, J. Highly efficient photocatalytic water splitting over edge-modified phosphorene nanoribbons. *J. Am. Chem. Soc.* **2017**, *139* (43), 15429−15436.
(98) Xie, J.; Zhang, H.; Li, S.; Wang, R.; Sun, X.; Zhou, M.; Zhou, J.; Lou, X.; Xie, Y. Defect-Rich MoS_2 Ultrathin Nanosheets with Additional Active Edge Sites for Enhanced Electrocatalytic Hydrogen Evolution. *Adv. Mater.* **2013**, *25* (40), 5807−5813.
(99) Zhang, X.; Li, N.; Wu, J.; Zheng, Y.; Tao, X. Defect-rich O-incorporated 1T-MoS_2 nanosheets for remarkably enhanced visible-light photocatalytic H_2 evolution over CdS: The impact of enriched defects. *Appl. Catal., B* **2018**, *229*, 227−236.
(100) Ding, Q.; Song, B.; Xu, P.; Jin, S. Efficient Electrocatalytic and Photoelectrochemical Hydrogen Generation Using MoS_2 and Related Compounds. *Chem.* **2016**, *1* (5), 699−726.
(101) Maitra, U.; Gupta, U.; De, M.; Datta, R.; Govindaraj, A.; Rao, C. Highly Effective Visible-Light-Induced H_2 Generation by Single-Layer 1T-MoS_2 and a Nanocomposite of Few-Layer 2H-MoS_2 with Heavily Nitrogenated Graphene. *Angew. Chem., Int. Ed.* **2013**, *52* (49), 13057−13061.
(102) Hao, X.; Zhou, J.; Cui, Z.; Wang, Y.; Wang, Y.; Zou, Z. Zn-vacancy mediated electron-hole separation in ZnS/g-C_3N_4 heterojunction for efficient visible-light photocatalytic hydrogen production. *Appl. Catal., B* **2018**, *229*, 41−51.
(103) Pilarski, M.; Marschall, R.; Gross, S.; Wark, M. Layered cesium copper titanate for photocatalytic hydrogen production. *Appl. Catal., B* **2018**, *227*, 349−355.
(104) Zhang, S.; Liu, X.; Liu, C.; Luo, S.; Wang, L.; Cai, T.; Zeng, Y.; Yuan, J.; Dong, W.; Pei, Y.; Liu, Y. MoS_2 Quantum Dot Growth Induced by S Vacancies in a $ZnIn_2S_4$ Monolayer: Atomic-Level Heterostructure for Photocatalytic Hydrogen Production. *ACS Nano* **2018**, *12* (1), 751−758.
(105) Amani, M.; Burke, R. A.; Ji, X.; Zhao, P.; Lien, D.-H.; Taheri, P.; Ahn, G. H.; Kirya, D.; Ager, J. W., III; Yablonovitch, E.; et al. High luminescence efficiency in MoS_2 grown by chemical vapor deposition. *ACS Nano* **2016**, *10* (7), 6535−6541.
(106) Yu, Y.; Yu, Y.; Xu, C.; Cai, Y. Q.; Su, L.; Zhang, Y.; Zhang, Y. W.; Gundogdu, K.; Cao, L. Engineering Substrate Interactions for High Luminescence Efficiency of Transition-Metal Dichalcogenide Monolayers. *Adv. Funct. Mater.* **2016**, *26* (26), 4733−4739.
(107) Zhao, W.; Ghorannevis, Z.; Chu, L.; Toh, M.; Kloc, C.; Tan, P.-H.; Eda, G. Evolution of electronic structure in atomically thin sheets of WS_2 and WSe_2. *ACS Nano* **2013**, *7* (1), 791−797.
(108) Tongay, S.; Zhou, J.; Ataca, C.; Lo, K.; Matthews, T. S.; Li, J.; Grossman, J. C.; Wu, J. Thermally driven crossover from indirect toward direct bandgap in 2D semiconductors: $MoSe_2$ versus MoS_2. *Nano Lett.* **2012**, *12* (11), 5576−5580.
(109) Bernardi, M.; Palummo, M.; Grossman, J. C. Extraordinary sunlight absorption and one nanometer thick photovoltaics using two-dimensional monolayer materials. *Nano Lett.* **2013**, *13* (8), 3664−3670.
(110) Chhowalla, M.; Shin, H. S.; Eda, G.; Li, L.-J.; Loh, K. P.; Zhang, H. The chemistry of two-dimensional layered transition metal dichalcogenide nanosheets. *Nat. Chem.* **2013**, *5* (4), 263.
(111) Gao, M.-R.; Xu, Y.-F.; Jiang, J.; Yu, S.-H. Nanostructured metal chalcogenides: synthesis, modification, and applications in energy conversion and storage devices. *Chem. Soc. Rev.* **2013**, *42* (7), 2986−3017.
(112) Jariwala, D.; Sangwan, V. K.; Lauhon, L. J.; Marks, T. J.; Hersam, M. C. Emerging device applications for semiconducting two-dimensional transition metal dichalcogenides. *ACS Nano* **2014**, *8* (2), 1102−1120.

DOI: 10.1021/acsenergylett.9b00940
ACS Energy Lett. 2019, 4, 1687−1709

(113) Lai, C.-H.; Lu, M.-Y.; Chen, L.-J. Metal sulfide nanostructures: synthesis, properties and applications in energy conversion and storage. *J. Mater. Chem.* **2012**, *22* (1), 19−30.
(114) Lv, R.; Robinson, J. A.; Schaak, R. E.; Sun, D.; Sun, Y.; Mallouk, T. E.; Terrones, M. Transition metal dichalcogenides and beyond: synthesis, properties, and applications of single-and few-layer nanosheets. *Acc. Chem. Res.* **2015**, *48* (1), 56−64.
(115) Pumera, M.; Sofer, Z.; Ambrosi, A. Layered transition metal dichalcogenides for electrochemical energy generation and storage. *J. Mater. Chem. A* **2014**, *2* (24), 8981−8987.
(116) Siahrostami, S.; Tsai, C.; Karamad, M.; Koitz, R.; García-Melchor, M.; Bajdich, M.; Vojvodic, A.; Abild-Pedersen, F.; Nørskov, J. K.; Studt, F. Two-dimensional materials as catalysts for energy conversion. *Catal. Lett.* **2016**, *146* (10), 1917−1921.
(117) Wang, H.; Feng, H.; Li, J. Graphene and graphene-like layered transition metal dichalcogenides in energy conversion and storage. *Small* **2014**, *10* (11), 2165−2181.
(118) Yu, X.; Sivula, K. Toward large-area solar energy conversion with semiconducting 2D transition metal dichalcogenides. *ACS Energy Letters* **2016**, *1* (1), 315−322.
(119) Salehzadeh, O.; Tran, N.; Liu, X.; Shih, I.; Mi, Z. Exciton kinetics, quantum efficiency, and efficiency droop of monolayer MoS_2 light-emitting devices. *Nano Lett.* **2014**, *14* (7), 4125−4130.
(120) Sun, D.; Rao, Y.; Reider, G. A.; Chen, G.; You, Y.; Brezin, L.; Harutyunyan, A. R.; Heinz, T. F. Observation of rapid exciton−exciton annihilation in monolayer molybdenum disulfide. *Nano Lett.* **2014**, *14* (10), 5625−5629.
(121) Wang, H.; Zhang, C.; Chan, W.; Manolatou, C.; Tiwari, S.; Rana, F. Radiative lifetimes of excitons and trions in monolayers of the metal dichalcogenide MoS_2. *Phys. Rev. B: Condens. Matter Mater. Phys.* **2016**, *93* (4), 045407.
(122) Yuan, L.; Huang, L. Exciton dynamics and annihilation in WS_2 2D semiconductors. *Nanoscale* **2015**, *7* (16), 7402−7408.
(123) Fang, H.; Battaglia, C.; Carraro, C.; Nemsak, S.; Ozdol, B.; Kang, J. S.; Bechtel, H. A.; Desai, S. B.; Kronast, F.; Unal, A. A.; et al. Strong interlayer coupling in van der Waals heterostructures built from single-layer chalcogenides. *Proc. Natl. Acad. Sci. U. S. A.* **2014**, *111* (17), 6198−6202.
(124) Lee, C.-H.; Lee, G.-H.; Van Der Zande, A. M.; Chen, W.; Li, Y.; Han, M.; Cui, X.; Arefe, G.; Nuckolls, C.; Heinz, T. F.; et al. Atomically thin p−n junctions with van der Waals heterointerfaces. *Nat. Nanotechnol.* **2014**, *9* (9), 676.
(125) Chen, K.; Wan, X.; Wen, J.; Xie, W.; Kang, Z.; Zeng, X.; Chen, H.; Xu, J.-B. Electronic properties of MoS_2−WS_2 heterostructures synthesized with two-step lateral epitaxial strategy. *ACS Nano* **2015**, *9* (10), 9868−9876.
(126) Duan, X.; Wang, C.; Shaw, J. C.; Cheng, R.; Chen, Y.; Li, H.; Wu, X.; Tang, Y.; Zhang, Q.; Pan, A.; et al. Lateral epitaxial growth of two-dimensional layered semiconductor heterojunctions. *Nat. Nanotechnol.* **2014**, *9* (12), 1024.
(127) Gong, Y.; Lin, J.; Wang, X.; Shi, G.; Lei, S.; Lin, Z.; Zou, X.; Ye, G.; Vajtai, R.; Yakobson, B. I.; et al. Vertical and in-plane heterostructures from WS_2/MoS_2 monolayers. *Nat. Mater.* **2014**, *13* (12), 1135.
(128) Huang, C.; Wu, S.; Sanchez, A. M.; Peters, J. J.; Beanland, R.; Ross, J. S.; Rivera, P.; Yao, W.; Cobden, D. H.; Xu, X. Lateral heterojunctions within monolayer $MoSe_2$−WSe_2 semiconductors. *Nat. Mater.* **2014**, *13* (12), 1096.
(129) Zhang, X.-Q.; Lin, C.-H.; Tseng, Y.-W.; Huang, K.-H.; Lee, Y.-H. Synthesis of lateral heterostructures of semiconducting atomic layers. *Nano Lett.* **2015**, *15* (1), 410−415.
(130) Li, M.-Y.; Shi, Y.; Cheng, C.-C.; Lu, L.-S.; Lin, Y.-C.; Tang, H.-L.; Tsai, M.-L.; Chu, C.-W.; Wei, K.-H.; He, J.-H.; et al. Epitaxial growth of a monolayer WSe_2-MoS_2 lateral p−n junction with an atomically sharp interface. *Science* **2015**, *349* (6247), 524−528.
(131) Cao, Z.; Harb, M.; Lardhi, S.; Cavallo, L. Impact of interfacial defects on the properties of monolayer transition metal dichalcogenide lateral heterojunctions. *J. Phys. Chem. Lett.* **2017**, *8* (7), 1664−1669.
(132) Heyd, J.; Scuseria, G. E.; Ernzerhof, M. Hybrid functionals based on a screened Coulomb potential. *J. Chem. Phys.* **2003**, *118* (18), 8207−8215.
(133) Steiner, S.; Khmelevskyi, S.; Marsmann, M.; Kresse, G. Calculation of the magnetic anisotropy with projected-augmented-wave methodology and the case study of disordered $Fe_{1-x}Co_x$ alloys. *Phys. Rev. B: Condens. Matter Mater. Phys.* **2016**, *93* (22), 224425.
(134) Bertolazzi, S.; Gobbi, M.; Zhao, Y.; Backes, C.; Samorì, P. Molecular chemistry approaches for tuning the properties of two-dimensional transition metal dichalcogenides. *Chem. Soc. Rev.* **2018**, *47* (17), 6845−6888.
(135) Zhang, Z.; Qian, Q.; Li, B.; Chen, K. Interface Engineering of Monolayer MoS2/GaN Hybrid Heterostructure: Modified Band Alignment for Photocatalytic Water Splitting Application by Nitridation Treatment. *ACS Appl. Mater. Interfaces* **2018**, *10* (20), 17419−17426.
(136) Bie, C.; Fu, J.; Cheng, B.; Zhang, L. Ultrathin CdS nanosheets with tunable thickness and efficient photocatalytic hydrogen generation. *Appl. Surf. Sci.* **2018**, *462*, 606−614.
(137) Shi, J.; Islam, I. U.; Chen, W.; Wang, F.; Xu, Z.; Xu, S.; Li, Y.; Lu, J. Two-dimensional ultrathin $Zn_xCd_{1-x}S$ nanosheet with exposed polar facet by using layered double hydroxide template for photocatalytic hydrogen generation. *Int. J. Hydrogen Energy* **2018**, *43* (42), 19481−19491.
(138) Yuan, H.; Han, K.; Dubbink, D.; Mul, G.; ten Elshof, J. E. Modulating the External Facets of Functional Nanocrystals Enabled by Two-Dimensional Oxide Crystal Templates. *ACS Catal.* **2017**, *7* (10), 6858−6863.
(139) Li, H.; Li, Y.; Aljarb, A.; Shi, Y.; Li, L.-J. Epitaxial growth of two-dimensional layered transition-metal dichalcogenides: growth mechanism, controllability, and scalability. *Chem. Rev.* **2018**, *118* (13), 6134−6150.
(140) Huang, Y. L.; Chen, Y.; Zhang, W.; Quek, S. Y.; Chen, C.-H.; Li, L.-J.; Hsu, W.-T.; Chang, W.-H.; Zheng, Y. J.; Chen, W.; et al. Bandgap tunability at single-layer molybdenum disulphide grain boundaries. *Nat. Commun.* **2015**, *6*, 6298.
(141) Aljarb, A.; Cao, Z.; Tang, H.-L.; Huang, J.-K.; Li, M.; Hu, W.; Cavallo, L.; Li, L.-J. Substrate Lattice-Guided Seed Formation Controls the Orientation of 2D Transition-Metal Dichalcogenides. *ACS Nano* **2017**, *11* (9), 9215−9222.
(142) Najmaei, S.; Amani, M.; Chin, M. L.; Liu, Z.; Birdwell, A. G.; O'Regan, T. P.; Ajayan, P. M.; Dubey, M.; Lou, J. Electrical transport properties of polycrystalline monolayer molybdenum disulfide. *ACS Nano* **2014**, *8* (8), 7930−7937.
(143) Wang, X.; Shen, X.; Wang, Z.; Yu, R.; Chen, L. Atomic-scale clarification of structural transition of MoS2 upon sodium intercalation. *ACS Nano* **2014**, *8* (11), 11394−11400.
(144) Nasr Esfahani, D.; Leenaerts, O.; Sahin, H.; Partoens, B.; Peeters, F. Structural transitions in monolayer MoS2 by lithium adsorption. *J. Phys. Chem. C* **2015**, *119* (19), 10602−10609.
(145) Hong, S.; Kumar, D.; Kim, E.; Park, H.; Gopannagari, M.; Reddy, D.; Kim, T. Earth abundant transition metal-doped few-layered MoS2 nanosheets on CdS nanorods for ultra-efficient photocatalytic hydrogen production. *J. Mater. Chem. A* **2017**, *5* (39), 20851−20859.
(146) Guo, Y.; Xu, K.; Wu, C.; Zhao, J.; Xie, Y. Surface chemical-modification for engineering the intrinsic physical properties of inorganic two-dimensional nanomaterials. *Chem. Soc. Rev.* **2015**, *44* (3), 637−646.
(147) Lin, C.; Zhu, X.; Feng, J.; Wu, C.; Hu, S.; Peng, J.; Guo, Y.; Peng, L.; Zhao, J.; Huang, J.; et al. Hydrogen-incorporated TiS_2 ultrathin nanosheets with ultrahigh conductivity for stamp-transferrable electrodes. *J. Am. Chem. Soc.* **2013**, *135* (13), 5144−5151.
(148) Feng, J.; Peng, L.; Wu, C.; Sun, X.; Hu, S.; Lin, C.; Dai, J.; Yang, J.; Xie, Y. Giant moisture responsiveness of VS_2 ultrathin nanosheets for novel touchless positioning interface. *Adv. Mater.* **2012**, *24* (15), 1969−1974.
(149) Xie, J.; Zhang, J.; Li, S.; Grote, F.; Zhang, X.; Zhang, H.; Wang, R.; Lei, Y.; Pan, B.; Xie, Y. Controllable disorder engineering in

DOI: 10.1021/acsenergylett.9b00940
ACS Energy Lett. 2019, 4, 1687−1709

oxygen-incorporated MoS_2 ultrathin nanosheets for efficient hydrogen evolution. *J. Am. Chem. Soc.* **2013**, *135* (47), 17881−17888.
(150) Chen, Z.; Xia, K.; She, X.; Mo, Z.; Zhao, S.; Yi, J.; Xu, Y.; Chen, H.; Xu, H.; Li, H. 1D metallic MoO_2 C as co-catalyst on 2D g-C_3N_4 semiconductor to promote photocatlaytic hydrogen production. *Appl. Surf. Sci.* **2018**, *447*, 732−739.
(151) Li, Z.; Yang, Y.; Dai, K.; Zhang, J.; Lu, L. Construction of defective $Mo_{15}S_{19}$/CdS-diethylenetriamine heterosctructure photocatalyst for highly active and stable noble-metal-free photocatalytic hydrogen production. *Appl. Surf. Sci.* **2018**, *469*, 505.
(152) Li, J.; Peng, Y.; Qian, X.; Lin, J. Few-layer Co-doped MoS_2 nanosheets with rich active sites as an efficient cocatalyst for photocatalytic H_2 production over CdS. *Appl. Surf. Sci.* **2018**, *452*, 437−442.
(153) Chen, J.; Wu, X.; Yin, L.; Li, B.; Hong, X.; Fan, Z.; Chen, B.; Xue, C.; Zhang, H. One-pot Synthesis of CdS Nanocrystals Hybridized with Single-Layer Transition-Metal Dichalcogenide Nanosheets for Efficient Photocatalytic Hydrogen Evolution. *Angew. Chem., Int. Ed.* **2015**, *54* (4), 1210−1214.
(154) Li, Q.; Zhou, B.; McBride, J.; Lian, T. Efficient Diffusive Transport of Hot and Cold Excitons in Colloidal Type II CdSe/CdTe Core/Crown Nanoplatelet Heterostructures. *ACS Energy Letters* **2017**, *2* (1), 174−181.
(155) Li, Q.; Wu, K.; Chen, J.; Chen, Z.; McBride, J.; Lian, T. Size-Independent Exciton Localization Efficiency in Colloidal CdSe/CdS Core/Crown Nanosheet Type-I Heterostructures. *ACS Nano* **2016**, *10* (3), 3843−3851.
(156) Li, Q.; Lian, T. Exciton dissociation dynamics and light-driven H-2 generation in colloidal 2D cadmium chalcogenide nanoplatelet heterostructures. *Nano Res.* **2018**, *11* (6), 3031−3049.
(157) Nasilowski, M.; Mahler, B.; Lhuillier, E.; Ithurria, S.; Dubertret, B. Two-Dimensional Colloidal Nanocrystals. *Chem. Rev.* **2016**, *116* (18), 10934−10982.
(158) Wu, K.; Li, Q.; Jia, Y.; McBride, J.; Xie, Z.; Lian, T. Efficient and Ultrafast Formation of Long-Lived Charge-Transfer Exciton State in Atomically Thin Cadmium Selenide/Cadmium Telluride Type-II Heteronanosheets. *ACS Nano* **2015**, *9* (1), 961−968.
(159) Li, Q.; Xu, Z.; McBride, J.; Lian, T. Low Threshold Multiexciton Optical Gain in Colloidal CdSe/CdTe Core/Crown Type-II Nanoplatelet Heterostructures. *ACS Nano* **2017**, *11* (3), 2545−2553.
(160) Simon, T.; Bouchonville, N.; Berr, M.; Vaneski, A.; Adrovic, A.; Volbers, D.; Wyrwich, R.; Doblinger, M.; Susha, A.; Rogach, A.; Jackel, F.; Stolarczyk, J.; Feldmann, J. Redox shuttle mechanism enhances photocatalytic H_2 generation on Ni-decorated CdS nanorods. *Nat. Mater.* **2014**, *13* (11), 1013−1018.
(161) Han, Z.; Qiu, F.; Eisenberg, R.; Holland, P.; Krauss, T. Robust Photogeneration of H_2 in Water Using Semiconductor Nanocrystals and a Nickel Catalyst. *Science* **2012**, *338* (6112), 1321−1324.
(162) Zhukovskyi, M.; Tongying, P.; Yashan, H.; Wang, Y.; Kuno, M. Efficient Photocatalytic Hydrogen Generation from Ni Nanoparticle Decorated CdS Nanosheets. *ACS Catal.* **2015**, *5* (11), 6615−6623.
(163) Xie, Y.; Zheng, Y.; Yang, Y.; Jiang, R.; Wang, G.; Zhang, Y.; Zhang, E.; Zhao, L.; Duan, C. Two-dimensional nickel hydroxide/sulfides nanosheet as an efficient cocatalyst for photocatalytic H_2 evolution over CdS nanospheres. *J. Colloid Interface Sci.* **2018**, *514*, 634−641.
(164) Jain, R.; Narayan, R.; Sasikala, S. P.; Lee, K. E.; Jung, H. J.; Kim, S. O. Phosphorene for energy and catalytic application—filling the gap between graphene and 2D metal chalcogenides. *2D Mater.* **2017**, *4* (4), 042006.
(165) Dou, Y.; Zhang, L.; Xu, X.; Sun, Z.; Liao, T.; Dou, S. X. Atomically thin non-layered nanomaterials for energy storage and conversion. *Chem. Soc. Rev.* **2017**, *46* (23), 7338−7373.
(166) Seh, Z. W.; Fredrickson, K. D.; Anasori, B.; Kibsgaard, J.; Strickler, A. L.; Lukatskaya, M. R.; Gogotsi, Y.; Jaramillo, T. F.; Vojvodic, A. Two-dimensional molybdenum carbide (MXene) as an efficient electrocatalyst for hydrogen evolution. *ACS Energy Letters* **2016**, *1* (3), 589−594.
(167) Cheng, Z.; Shifa, T.; Wang, F.; Gao, Y.; He, P.; Zhang, K.; Jiang, C.; Liu, Q.; He, J. High-Yield Production of Monolayer $FePS_3$ Quantum Sheets via Chemical Exfoliation for Efficient Photocatalytic Hydrogen Evolution. *Adv. Mater.* **2018**, *30* (26), 1707433.
(168) Pang, J.; Mendes, R. G.; Bachmatiuk, A.; Zhao, L.; Ta, H. Q.; Gemming, T.; Liu, H.; Liu, Z.; Rummeli, M. H. Applications of 2D MXenes in energy conversion and storage systems. *Chem. Soc. Rev.* **2019**, *48* (1), 72−133.
(169) Li, P.; Zhu, J.; Handoko, A. D.; Zhang, R.; Wang, H.; Legut, D.; Wen, X.; Fu, Z.; Seh, Z. W.; Zhang, Q. High-throughput theoretical optimization of the hydrogen evolution reaction on MXenes by transition metal modification. *J. Mater. Chem. A* **2018**, *6* (10), 4271−4278.
(170) Halim, J.; Lukatskaya, M.; Cook, K.; Lu, J.; Smith, C.; Naslund, L.; May, S.; Hultman, L.; Gogotsi, Y.; Eklund, P.; Barsoum, M. Transparent Conductive Two-Dimensional Titanium Carbide Epitaxial Thin Films. *Chem. Mater.* **2014**, *26* (7), 2374−2381.
(171) Anasori, B.; Xie, Y.; Beidaghi, M.; Lu, J.; Hosler, B.; Hultman, L.; Kent, P.; Gogotsi, Y.; Barsoum, M. Two-Dimensional, Ordered, Double Transition Metals Carbides (MXenes). *ACS Nano* **2015**, *9* (10), 9507−9516.
(172) Naguib, M.; Gogotsi, Y. Synthesis of Two-Dimensional Materials by Selective Extraction. *Acc. Chem. Res.* **2015**, *48* (1), 128−135.
(173) Yuan, W.; Cheng, L.; An, Y.; Lv, S.; Wu, H.; Fan, X.; Zhang, Y.; Guo, X.; Tang, J. Laminated Hybrid Junction of Sulfur-Doped TiO_2 and a Carbon Substrate Derived from Ti_3C_2 MXenes: Toward Highly Visible Light-Driven Photocatalytic Hydrogen Evolution. *Advanced Science* **2018**, *5* (6), 1700870.
(174) Sun, Y.; Jin, D.; Sun, Y.; Meng, X.; Gao, Y.; Dall'Agnese, Y.; Chen, G.; Wang, X. g-C_3N_4/$Ti_3C_2T_x$ (MXenes) composite with oxidized surface groups for efficient photocatalytic hydrogen evolution. *J. Mater. Chem. A* **2018**, *6* (19), 9124−9131.
(175) Su, T.; Peng, R.; Hood, Z.; Naguib, M.; Ivanov, I.; Keum, J.; Qin, Z.; Guo, Z.; Wu, Z. One-Step Synthesis of Nb_2O_5/C/Nb_2C (MXene) Composites and Their Use as Photocatalysts for Hydrogen Evolution. *ChemSusChem* **2018**, *11* (4), 688−699.
(176) Ran, J.; Gao, G.; Li, F.-T.; Ma, T.-Y.; Du, A.; Qiao, S.-Z. Ti_3C_2 MXene co-catalyst on metal sulfide photo-absorbers for enhanced visible-light photocatalytic hydrogen production. *Nat. Commun.* **2017**, *8*, 13907.
(177) Chen, X.; Sun, X.; Xu, W.; Pan, G.; Zhou, D.; Zhu, J.; Wang, H.; Bai, X.; Dong, B.; Song, H. Ratiometric photoluminescence sensing based on Ti_3C_2 MXene quantum dots as an intracellular pH sensor. *Nanoscale* **2018**, *10* (3), 1111−1118.
(178) Peng, C.; Wei, P.; Li, X.; Liu, Y.; Cao, Y.; Wang, H.; Yu, H.; Peng, F.; Zhang, L.; Zhang, B.; et al. High efficiency photocatalytic hydrogen production over ternary Cu/TiO_2@ $Ti_3C_2T_x$ enabled by low-work-function 2D titanium carbide. *Nano Energy* **2018**, *53*, 97−107.
(179) Wulan, B.; Yi, S.; Li, S.; Duan, Y.; Yan, J.; Jiang, Q. Amorphous nickel pyrophosphate modified graphitic carbon nitride: an efficient photocatalyst for hydrogen generation from water splitting. *Appl. Catal., B* **2018**, *231*, 43−50.
(180) Kong, L.; Ji, Y.; Dang, Z.; Yan, J.; Li, P.; Li, Y.; Liu, S. g-C_3N_4 Loading Black Phosphorus Quantum Dot for Efficient and Stable Photocatalytic H_2 Generation under Visible Light. *Adv. Funct. Mater.* **2018**, *28* (22), 1800668.
(181) Meng, N.; Ren, J.; Liu, Y.; Huang, Y.; Petit, T.; Zhang, B. Engineering oxygen-containing and amino groups into two-dimensional atomically-thin porous polymeric carbon nitrogen for enhanced photocatalytic hydrogen production. *Energy Environ. Sci.* **2018**, *11* (3), 566−571.
(182) Zeng, D.; Xu, W.; Ong, W.; Xu, J.; Ren, H.; Chen, Y.; Zheng, H.; Peng, D. Toward noble-metal-free visible-light-driven photocatalytic hydrogen evolution: Monodisperse sub-15 nm Ni2P

DOI: 10.1021/acsenergylett.9b00940
ACS Energy Lett. 2019, 4, 1687−1709

nanoparticles anchored on porous g-C_3N_4 nanosheets to engineer 0D-2D heterojunction interfaces. *Appl. Catal., B* **2018**, *221*, 47−55.
(183) He, Z.; Kim, C.; Lin, L.; Jeon, T.; Lin, S.; Wang, X.; Choi, W. Formation of heterostructures via direct growth CN on h-BN porous nanosheets for metal-free photocatalysis. *Nano Energy* **2017**, *42*, 58−68.
(184) Wu, K.; Huang, Y.; Teng, H. Oligomer-Incorporated Polymeric Layer Framework of Graphitic Carbon Nitride for Effective Photocatalytic Hydrogen Evolution. *Particle & Particle Systems Characterization* **2018**, *35* (1), 1700221.
(185) Cai, X.; Zhang, J.; Fujitsuka, M.; Majima, T. Graphitic-C_3N_4 hybridized N-doped $La_2Ti_2O_7$ two-dimensional layered composites as efficient visible-light-driven photocatalyst. *Appl. Catal., B* **2017**, *202*, 191−198.
(186) Chen, X.; Chen, H.; Guan, J.; Zhen, J.; Sun, Z.; Du, P.; Lu, Y.; Yang, S. A facile mechanochemical route to a covalently bonded graphitic carbon nitride (g-C_3N_4) and fullerene hybrid toward enhanced visible light photocatalytic hydrogen production. *Nanoscale* **2017**, *9* (17), 5615−5623.
(187) Lin, B.; Li, H.; An, H.; Hao, W.; Wei, J.; Dai, Y.; Ma, C.; Yang, G. Preparation of 2D/2D g-C_3N_4 nanosheet@ $ZnIn_2S_4$ nanoleaf heterojunctions with well-designed high-speed charge transfer nanochannels towards high-efficiency photocatalytic hydrogen evolution. *Appl. Catal., B* **2018**, *220*, 542−552.
(188) Gomes Silva, C.; Luz, I.; Llabres i Xamena, F. X.; Corma, A.; Garcia, H. Water Stable Zr-Benzenedicarboxylate Metal-Organic Frameworks as Photocatalysts for Hydrogen Generation. *Chem.—Eur. J.* **2010**, *16* (36), 11133−11138.
(189) Horiuchi, Y.; Toyao, T.; Saito, M.; Mochizuki, K.; Iwata, M.; Higashimura, H.; Anpo, M.; Matsuoka, M. Visible-Light-Promoted Photocatalytic Hydrogen Production by Using an Amino-Functionalized Ti(IV) Metal-Organic Framework. *J. Phys. Chem. C* **2012**, *116* (39), 20848−20853.
(190) He, J.; Yan, Z.; Wang, J.; Xie, J.; Jiang, L.; Shi, Y.; Yuan, F.; Yu, F.; Sun, Y. Significantly enhanced photocatalytic hydrogen evolution under visible light over CdS embedded on metal-organic frameworks. *Chem. Commun.* **2013**, *49* (60), 6761−6763.
(191) Shen, L.; Luo, M.; Huang, L.; Feng, P.; Wu, L. A Clean and General Strategy To Decorate a Titanium Metal Organic Framework with Noble-Metal Nanoparticles for Versatile Photocatalytic Applications. *Inorg. Chem.* **2015**, *54* (4), 1191−1193.
(192) Tilgner, D.; Kempe, R. A Plasmonic Colloidal Photocatalyst Composed of a Metal-Organic Framework Core and a Gold/Anatase Shell for Visible-Light-Driven Wastewater Purification from Antibiotics and Hydrogen Evolution. *Chem. - Eur. J.* **2017**, *23* (13), 3184−3190.
(193) Gao, H.; Zhen, W.; Ma, J.; Lu, G. High efficient solar hydrogen generation by modulation of Co-Ni sulfide (220) surface structure and adjusting adsorption hydrogen energy. *Appl. Catal., B* **2017**, *206*, 353−363.
(194) Nishino, H.; Fujita, T.; Cuong, N. T.; Tominaka, S.; Miyauchi, M.; Iimura, S.; Hirata, A.; Umezawa, N.; Okada, S.; Nishibori, E.; et al. Formation and characterization of hydrogen boride sheets derived from MgB2 by cation exchange. *J. Am. Chem. Soc.* **2017**, *139* (39), 13761−13769.
(195) Ida, S.; Takashiba, A.; Koga, S.; Hagiwara, H.; Ishihara, T. Potential Gradient and Photocatalytic Activity of an Ultrathin p-n Junction Surface Prepared with Two-Dimensional Semiconducting Nanocrystals. *J. Am. Chem. Soc.* **2014**, *136* (5), 1872−1878.
(196) Okamoto, Y.; Ida, S.; Hyodo, J.; Hagiwara, H.; Ishihara, T. Synthesis and Photocatalytic Activity of Rhodium-Doped Calcium Niobate Nanosheets for Hydrogen Production from a Water/Methanol System without Cocatalyst Loading. *J. Am. Chem. Soc.* **2011**, *133* (45), 18034−18037.
(197) Guan, Z.; Xu, Z.; Li, Q.; Wang, P.; Li, G.; Yang, J. AgIn5S8 nanoparticles anchored on 2D layered ZnIn2S4 to form OD/2D heterojunction for enhanced visible-light photocatalytic hydrogen evolution. *Appl. Catal., B* **2018**, *227*, 512−518.
(198) Kong, X.; Xu, Y.; Cui, Z.; Li, Z.; Liang, Y.; Gao, Z.; Zhu, S.; Yang, X. Defect enhances photocatalytic activity of ultrathin TiO2 (B) nanosheets for hydrogen production by plasma engraving method. *Appl. Catal., B* **2018**, *230*, 11−17.
(199) Wang, Y.; Liu, Y.; Zhang, J.; Wu, J.; Xu, H.; Wen, X.; Zhang, X.; Tiwary, C. S.; Yang, W.; Vajtai, R.; et al. Cryo-mediated exfoliation and fracturing of layered materials into 2D quantum dots. *Science Advances* **2017**, *3* (12), e1701500.
(200) Wen, H.; Li, H.; He, S.; Chen, F.; Ding, E.; Liu, S.; Wang, B.; Peng, Y. Constructing two-dimensional CuFeSe2@Au heterostructured nanosheets with an amorphous core and a crystalline shell for enhanced near-infrared light water oxidation. *Nanoscale* **2018**, *10* (5), 2380−2387.
(201) Liao, C.-H.; Huang, C.-W.; Wu, J. Hydrogen production from semiconductor-based photocatalysis via water splitting. *Catalysts* **2012**, *2* (4), 490−516.
(202) Yang, L.; Li, X.; Zhang, G.; Cui, P.; Wang, X.; Jiang, X.; Zhao, J.; Luo, Y.; Jiang, J. Combining photocatalytic hydrogen generation and capsule storage in graphene based sandwich structures. *Nat. Commun.* **2017**, *8*, 16049.
(203) Zhang, H.; Tong, C.-J.; Zhang, Y.; Zhang, Y.-N.; Liu, L.-M. Porous BN for hydrogen generation and storage. *J. Mater. Chem. A* **2015**, *3* (18), 9632−9637.
(204) Serpone, N.; Emeline, A. Semiconductor Photocatalysis - Past, Present, and Future Outlook. *J. Phys. Chem. Lett.* **2012**, *3* (5), 673−677.

DOI: 10.1021/acsenergylett.9b00940
ACS Energy Lett. 2019, 4, 1687−1709